JOURNAL OF VIROLOGY, May 2006, p. 4801–4819 Vol. 80, No. 10
0022-538X/06/$08.00+0 doi:10.1128/JVI.80.10.4801–4819.2006

Lymphoma Cell Apoptosis in the Liver Induced by Distant Murine Cytomegalovirus Infection

Katja C. Erlach, Verena Böhm, Christof K. Seckert, Matthias J. Reddehase,* and Jürgen Podlech

Institute for Virology, Johannes Gutenberg-University, Mainz, Germany

Received 23 August 2005/Accepted 2 March 2006

Cytomegalovirus (CMV) poses a threat to the therapy of hematopoietic malignancies by hematopoietic stem cell transplantation, but efficient reconstitution of antiviral immunity prevents CMV organ disease. Tumor relapse originating from a minimal residual leukemia poses another threat. Although a combination of risk factors was supposed to enhance the incidence and severity of transplantation-associated disease, a murine model of a liver-adapted B-cell lymphoma has previously shown a survival benefit and tumor growth inhibition by nonlethal subcutaneous infection with murine CMV. Here we have investigated the underlying antitumoral mechanism. Virus replication proved to be required, since inactivated virions or the highly attenuated enhancerless mutant mCMV-ΔMIEenh did not impact the lymphoma in the liver. Surprisingly, the dissemination-deficient mutant mCMV-ΔM36 inhibited tumor growth, even though this virus fails to infect the liver. On the other hand, various strains of herpes simplex viruses consistently failed to control the lymphoma, even though they infect the liver. A quantitative analysis of the tumor growth kinetics identified a transient tumor remission by apoptosis as the antitumoral effector mechanism. Tumor cell colonies with cells surviving the CMV-induced "apoptotic crisis" lead to tumor relapse even in the presence of full-blown tissue infection. Serial transfer of surviving tumor cells did not indicate a selection of apoptosis-resistant genetic variants. NK cell activity of CD49b-expressing cells failed to control the lymphoma upon adoptive transfer. We propose the existence of an innate antitumoral mechanism that is triggered by CMV infection and involves an apoptotic signal effective at a distant site of tumor growth.

Complications of bone marrow transplantation (BMT) or hematopoietic stem cell transplantation include graft failure and graft-versus-host disease (46), infections, and minimal residual disease/leukemia giving rise to relapse of the initial tumor against which the hematoablative therapy was administered (12, 16, 21). Among infections in the immunocompromised BMT/hematopoietic stem cell transplantation recipients, human cytomegalovirus (hCMV) infection remains the most frequent and most severe (for recent reviews, see references 9, 17, and 33), despite antiviral therapy and although efficient reconstitution of antiviral immunity, of CD8 T cells in particular, can prevent lethal CMV organ disease in mouse models and in patients (for recent reviews, see references 22 and 34). While a wealth of literature separately deals either with tumor relapse or with CMV in clinical and experimental settings, information on an interference between CMV and tumors is scarce, except for a proposed role of hCMV genes in cell transformation (20, 57), a conspicuous association between hCMV and malignant gliomas (19), and an enhancement of tumor cell invasiveness by modulating the expression of adhesion molecules NCAM/CD56 and α5β1 integrin VLA-5 in persistently infected neuroblastoma cells (8, 63). Tumor-controlling properties of CMVs are currently even less of an issue, with the exception of a reported beneficial role for hCMV infection in adult T-cell leukemia/lymphoma (27, 28). This is somewhat surprising in view of the fact that CMVs have a broad cell-type tropism in vivo (52, 55) and are therefore likely to be cytopathogenic for tumor cells derived from various cell lineages.

In previous work, we have established an experimental model for studying the impact of CMV infection on a lymphoma under the conditions of hematoablative conditioning followed by BMT. Lymphoma E12E, a *lacZ*-transfected and liver-adapted clonal variant of B-cell lymphoma A20, was deliberately chosen as a tumor model that is not permissive for productive infection with murine CMV (mCMV) and not even permissive for the expression of the transactivating immediate-early (IE) proteins (24). Thus, by design, tumor remission by cytolytic infection of the tumor cells was excluded as an antitumoral mechanism. Surprisingly, mCMV infection nevertheless impressively suppressed the growth of the E12E lymphoma in the liver, resulting in a significant survival benefit in tumor-bearing and infected BMT recipients. While at first glance a CMV-triggered or -enhanced graft-versus-leukemia effect of innate immunity appeared to be a plausible mechanism, the finding that tumor inhibition by mCMV also operates after immunoablative treatment without reconstitution of immune cells through BMT—and moreover is not improved by BMT—rather argued against a primarily immunological mechanism. Induction of tumor cell apoptosis appeared to be excluded by the histological finding that tumor cells proliferated in the liver in close proximity to infected hepatocytes, as evidenced by mitotic figures, expression of proliferating cell nuclear antigen in all tumor cells, and absence of active caspase 3. Furthermore, tumor necrosis factor alpha (TNF-α) was shown not to be involved in the antitumoral effect either as a death receptor ligand or by its systemic effects on the endothelium (24). So, whereas the antitumoral effect of mCMV infection was highly reproducible and macroscopically evident

* Corresponding author. Mailing address: Institute for Virology, Johannes Gutenberg-University, Hochhaus am Augustusplatz, 55101 Mainz, Germany. Phone: 49-6131-39-33650. Fax: 49-6131-39-35604. E-mail: Matthias.Reddehase@uni-mainz.de.

from a considerably reduced tumor mass in the liver at later points of time, the underlying mechanism remained a difficult puzzle.

Progress reported here is based primarily on the dissemination-deficient virus mutant mCMV-ΔM36 (18, 48) as well as on a precise kinetics of tumor growth in the liver identifying the following three phases in the infected group. Phase I consisted of tumor cell extravasation, homing, and initial exponential growth until the four-cell stage, phase II consisted of transient remission by tumor cell apoptosis induced by distant mCMV infection, and phase III consisted of tumor relapse by exponential growth of surviving tumor cells in the presence of a full-blown liver infection. As a consequence of exponential growth, a minor reduction in the number of tumor cells by apoptosis in the early and transient remission phase, phase II, leads to a great absolute reduction in late tumor burden that confers a significant survival benefit.

MATERIALS AND METHODS

Tumor models. (i) B-cell lymphoma. The E12E lymphoma (24) is a *lacZ*-transfected, liver-adapted clonal variant of the BALB/c (*H-2*^{d})-derived B-cell lymphoma A20, ATCC TIB-208 (41). In immunocompromised BALB/c mice, the highly invasive parental A20 lymphoma colonizes the intestine, spleen, liver, lungs and bone marrow and destructively infiltrates retroperitoneal tissue, paravertebral musculature, and the spinal cord, resulting in paralysis of the hind limbs. In contrast, its variant E12E colonizes the liver almost exclusively and is generally less aggressive. However, in immunocompetent or in immunocompromised BALB/c mice reconstituted by syngeneic BMT, E12E is less immunogenic and hence more tumorigenic than A20. Briefly, A20 cells were transfected, resulting in the cell line A20-*lacZ*, and, by limiting dilution, 25 clones were selected on the basis of stable expression of the reporter gene. Clones were then passaged in vivo, and clone IID11 was selected for ex tumore recloning from a macroscopically visible liver metastasis. From 58 subclones, E12E was selected for further studies on the basis of liver tumorigenicity. E12E was frozen in passage 8 after recloning of IID11, and the passage 8 stock is used throughout for expansion to the cell number needed. E12E is not permissive for mCMV infection; it fails to express the IE1 protein, as evidenced by negative IE1-specific immunohistology in situ (24) and by negative IE1-specific immunofluorescence in cell culture (K. C. Erlach, unpublished).

(ii) T-cell lymphomas. Lymphomas ESb-MP and ESb-L-CI are variants of lymphoma ESb289, which is a highly metastatic subline of lymphoma Eb288 derived from T-cell lymphoma L5178Y/E, originally induced by methylcholanthren in DBA/2 (*H-2*^{d}) mice. ESb-MP is an attenuated, adhesion-selected variant of ESb (6). ESb-L-CI (clone 5) is a *lacZ*-transduced and highly aggressive, hepatotropic variant of ESb (39, 44). Like the B-cell lymphomas A20 and E12E, these two T-cell lymphomas express the cell surface antigen CD45R/B220 and are not permissive for mCMV infection.

Model 1. In a set of experiments, syngeneic BMT was performed with 8-week-old female BALB/c mice as bone marrow cell donors and recipients. Hematoablative conditioning of the recipients was performed by total-body γ irradiation with a dose of 7 Gy delivered by a ^{137}Cs gamma ray source 24 h prior to BMT (referred to as day −1). BMT was performed on day 0 with 10^7 donor femoral and tibial bone marrow cells administered intravenously (i.v.) in the tail vein of recipients. Indicated numbers of E12E lymphoma cells (10^4 to 10^6) were administered in a mixture with the bone marrow cells in a total volume of 0.5 ml of physiological saline. If not indicated otherwise, intraplantar infection was performed shortly after BMT and tumor cell transfer. Under these conditions of so-called "high-dose BMT," CMV disease and CMV-associated lethality are prevented by reconstitution of antiviral CD8 T cells (34).

Model 2. This model, used in most experiments, matches model 1 except that no BMT is performed, which results in lethal multiple-organ CMV disease, with death of all recipients occurring between day 10 and day 16. For greater technical detail, see the work of Podlech et al. (53).

Animal experiments were approved by the Ethics Commission, permission no. Az.177-07/021-29, according to German federal law. BALB/c mice were bred and housed under specific-pathogen-free conditions in the Central Laboratory Animal Facility (CLAF) of the Johannes Gutenberg-University, Mainz, Germany.

Quantitation of tumor cell proliferation in cell culture. E12E cells were seeded into 2-ml cultures (24-well flat-bottom culture plates, catalog no. 662102; Greiner Bio-One, Frickenhausen, Germany) at a density of 2×10^5 cells per ml in RPMI 1640 culture medium supplemented with 10% (vol/vol) fetal calf serum, 5×10^{-5} M 2-mercaptoethanol, 2 mM L-glutamine, 10 mM HEPES buffer (pH 7.2), 0.1 mg of streptomycin sulfate per ml, 100 U of penicillin per ml, and 1 mg of G418 sulfate (Geneticin, catalog no. 345810; Merck Biosciences) per ml.

Growth curves were determined by counting the cells in triplicate cultures first at 24 h after seeding and then in 12-h intervals until 84 h after seeding. Linear regression lines in a semilogarithmic plot of $\log n_t = at + \log n_0$, where n_t is the number of cells at time t after seeding, a is the slope of the regression line, and $\log n_0$ is the ordinate intercept of the regression line, were calculated by using Mathematica Statistics LinearRegression software, version 5.1 (Wolfram Research, Inc., Champaign, Ill.). The doubling time (DT) of the cells is then $\log 2/a$. Accordingly, the upper and lower 95% confidence limit values of slope a (determined from the ellipsoidal parameter confidence region) give the 95% confidence interval of the DT.

Quantitation of tumor cell extravasation and tumor growth in vivo. E12E, ESb-MP, and ESb-L-CI lymphoma cells were detected in deparaffinized 2-μm sections of liver tissue by immunohistochemical (IHC) labeling of the CD45R/B220 cell surface antigen using monoclonal antibody (MAb) RA3-6B2 and the avidin-biotin complex (ABC)–peroxidase diaminobenzidine (DAB)–nickel method for black staining, as described previously (24). At early points of time (up to day 7), tumor cells were counted under a microscope (Axiophot equipped with Plan-Neofluar oil immersion optics; Carl Zeiss Jena GmbH, Jena, Germany). At later time points (after day 7), areas covered by tumor noduli in the liver tissue sections were measured after digitalization of microphotographs by using the area morphometry utility of the analySIS software, version 3.0, for image analysis (Software Imaging Systems GmbH, Münster, Germany), as illustrated below (see Fig. 3) and described in greater detail previously (24).

Growth curves were determined by counting the stained E12E cells at daily intervals for individual recipients per time point. Linear regression lines in a semilogarithmic plot were calculated as described above for the growth curves in cell culture. Again, slope a of the regression line gives the DT as $\log 2/a$, and the upper and lower 95% confidence limit values of slope a give its 95% confidence interval. Importantly, the intercept of the regression line with the ordinate, $\log n_0$, and its upper and lower 95% confidence limit values (determined from the ellipsoidal parameter confidence region) give the transmigration rate, that is, the number of tumor cells that have migrated through the endothelium for homing in the liver, as $\text{delog}\, n_0$ and its 95% confidence interval.

Viruses. All viruses were cell culture propagated and sucrose gradient purified as described in greater detail previously (53). Strain Smith ATCC VR-194 of mCMV, recently reaccessioned as VR-1399, is here referred to as wild-type mCMV (mCMV-WT). Inactivated virions (mCMV-WT^{UV}) were generated from strain Smith virus by inactivation with 254-nm UV light. Inactivation was verified by absence of intranuclear IE1 protein expression in otherwise highly permissive murine embryofetal fibroblasts (MEF) inoculated with a dose that is equivalent to a multiplicity of infection of 4 PFU per cell. Mutant virus mCMV-IE1-L176A, in which antigenicity of the L^d-restricted IE1 peptide 168-YPHFMPTNL-176 (58, 59) is wiped out by point mutation of the C-terminal major histocompatibility complex (MHC) anchor residue Leu to Ala, as well as the corresponding revertant virus, mCMV-IE1-A176L, was kindly provided by C. O. Simon and N. K. A. Grzimek-Koschewa at our institute. Both recombinant viruses were shown to replicate in cell culture and in vivo like mCMV-WT (unpublished data). Deletion mutant mCMV-ΔM36 (48) was generously provided by the group of U. H. Koszinowski, Max von Pettenkofer Institute, Munich, Germany. mCMV-WT and the named mutants were propagated on MEF. The major IE (MIE) enhancer deletion mutant mCMV-C3XdE::Luc, here referred to as mCMV-ΔMIEenh, was generously provided by the group of A. Angulo and P. Ghazal, then at the Scripps Research Institute, La Jolla, Calif. This virus contains a 770-bp fragment from the luciferase gene as a stuffer sequence in place of the nucleotide sequence from −48 to −1191 of the mCMV MIE enhancer region (29). Efficient propagation of this enhancerless virus was performed with the complementing cell line NIH 3T3-Bam25 expressing the transactivator-encoding IE genes *ie1* and *ie3* (29). As mCMV-ΔMIEenh does not form easily countable plaques on NIH 3T3-Bam25 cells, genomes in the purified virus stock were quantitated by *M55*/*gB*-specific real-time quantitative PCR (see below), and doses for infection were defined by the number of genomes that equals the number of mCMV-WT genomes representing a defined infectivity measured as PFU. Specifically, 1 PFU of mCMV-WT represents ~397 (199 to 788) genomes (not shown), which is in fair accordance with previous data that were based on a direct Southern blot of virion DNA as well as on conventional PCR followed by Southern blot hybridization and phosphorimaging and which had estimated an

approximate genome-to-infectivity ratio of 500 for mCMV-WT (45) as well as for an enhancer swap mutant containing the hCMV MIE enhancer and promoter in place of the mCMV MIE enhancer and promoter (31). A comparable genome-to-infectivity ratio of mCMV-WT grown on MEF and mCMV-ΔMIEenh grown on NIH 3T3-Bam25 cells is strongly suggested by the comparable yield of viral genomes in the identically performed virus propagation and purification procedure that starts with a low multiplicity of infection of 0.01 (not shown). Strain Towne of hCMV was grown and quantitated for infectivity in primary cultures of human foreskin fibroblasts according to standard procedures. Herpes simplex virus (HSV) strains were grown and quantitated for infectivity on African green monkey kidney cells, Vero ATCC CCL-81.

ELISPOT assay for sensitive detection of viral peptide presentation. A gamma interferon (IFN-γ)-based enzyme-linked immunospot (ELISPOT) assay was performed essentially as described previously (35, 37), except that E12E lymphoma cells were used as peptide-presenting stimulator cells. In brief, log 2-graded numbers of effector cells in triplicate microcultures were incubated for ~18 h with 10^5 E12E cells that were either loaded with synthetic IE1 peptide at the indicated concentrations or exposed for 2 h prior to the assay to the indicated viruses at a dose of 4 PFU per cell. Effector cells were cytolytic T lymphocytes (CTL) of an IE1 epitope-specific but still polyclonal CTL line referred to as IE1-CTLL (51). Spots were counted and the frequencies of IFN-γ-secreting, spot-forming cells were calculated by intercept-free linear regression analysis as explained in greater detail previously (51).

Phenotypic and functional characterization of NK cells. (i) Cytofluorometric quantitation of NK cells. Lymph node (LN) cells derived from the draining popliteal lymph node after intraplantar infection were stained with fluorescein isothiocyanate (FITC)-conjugated MAb rat anti-mouse CD49b (clone DX5, catalog no. 553857; BD Pharmingen) and R-phycoerythrin-conjugated hamster MAb anti-mouse T-cell receptor (TCR) β chain (clone H57-597, catalog no. 553172; BD Pharmingen). Prior to the specific labeling, Fcγ III/II receptors were blocked by using purified anti-mouse CD16/CD32 MAb (clone 2.4G2, catalog no. 553142; BD Pharmingen; 1 μg per 10^6 cells in 100 μl of blocking solution) to avoid unspecific staining. The two-color cytofluorometric analysis was performed with a FACSort instrument (Becton Dickinson) using CellQuest software for data processing. Fluorescence channels 1 and 2 represent fluorescein fluorescence and phycoerythrin fluorescence, respectively.

(ii) Immunomagnetic negative sorting for depletion of NK cells. Lymph node cells were either labeled with FITC-conjugated rat anti-mouse CD49b (pan-NK cell) MAb DX5 {immunoglobulin M(κ) [IgM(κ)]} or incubated with FITC-conjugated rat IgM(κ) (clone R4-22, catalog no. 553942; BD Pharmingen) for isotype control. Automated magnetic cell sorting (AutoMACS system; Miltenyi Biotec Systems, Bergisch-Gladbach, Germany) was performed by using anti-fluorescein antibody-conjugated MicroBeads (catalog no. 130-048-701; Miltenyi) (20 μl per 10^7 cells) and the Possel separation program (Miltenyi) for one-column separation. Cells in the flowthrough were collected for functional analysis of CD49b-negative lymph node cells.

(iii) Cytolytic assay. The cytolytic activity of lymph node cells was tested in an 8-hour ^{51}Cr release assay with 10^3 ^{51}Cr-labeled target cells: E12E and the prototypic MHC class-I^{low} NK cell target YAC-1, a Moloney murine leukemia virus-induced lymphoma cell line (ATCC TIB-160).

Quantitation of viral genomes. Local virus replication in tissue at the site of subcutaneous/intraplantar infection as well as viremic dissemination was determined by quantitation of viral DNA using an *M55*/*gB*-specific real-time quantitative PCR with plasmid pDrive_gB_PTHrP_Tdy as a standard (65).

(i) Quantitation of viral DNA in whole-blood samples. As the cellularity in blood rapidly declines as a result of hematoablative γ irradiation, data for the viral sequence could not be normalized to the autosomal cellular *pthrp* gene (two copies in the diploid set of chromosomes). Instead, the number of viral copies was determined for a defined volume of whole blood. For each individual mouse tested ($n = 3$ per experimental group), 100 μl of whole blood was immediately mixed with 20 μl of EDTA (86 mM stock solution in distilled water) and 80 μl of phosphate-buffered saline (PBS) to reach a final sample volume of 200 μl. DNA was extracted using a QIAamp DNA Blood Mini kit (catalog no. 51106; QIAGEN) following the manufacturer's recommendations (manual 02/2003, blood and body fluid spin protocol). In brief, protease digestion was followed by DNA binding to the QIAamp spin column, two rounds of washing, and elution of DNA in a total volume of 100 μl. A 1/25 aliquot (4 μl) of the eluted DNA was used as the template in TaqMan PCR with a QuantiTect probe PCR kit (catalog no. 204343; QIAGEN). Reactions were performed in a total volume of 20 μl with an initial $MgCl_2$ concentration of 4 mM, 1 μM of each primer, and 0.25 μM of dually labeled probe. Primers for amplification of a 91-bp fragment of gene *M55*/*gB* were gB_Taq_For1 (5′-CTAGCTGTTTTAACGCGCGG) and gB_Taq_Rev1 (5′-GGTAAGGCGTGGACTAGCGAT), representing map positions from 83,137 to 83,156 and from 83,227 to 83,207, respectively (GenBank accession no. NC_004065 [complete mCMV Smith genome]). The probe gB_Taq_P1 {5′-[6-carboxyfluorescein (FAM)]TGCTCGGTGTAGGTCCTCTCCAAGCC[6-carboxytetramethylrhodamine-FAM]} represents map positions 83,175 to 83,200. Depletion of blood cells due to hematoablative γ irradiation was monitored by quantitation of the *pthrp* gene. Primers and probe for amplification of a 101-bp fragment were PTHrP_Taq_For1 (5′-CAAGGGCAAGTCCATCCAAG), PTHrP_Taq_Rev1 (5′-GGGACACCTCCGAGGTAGCT), and PTHrP_Taq_P1 (5′-[FAM]TTGC GCCGCCGTTTCTTCCTC[6-carboxytetramethylrhodamine-FAM]), representing map positions from 155 to 174, from 255 to 236, and from 177 to 197, respectively (GenBank accession no. M60056). Two-step PCR was performed with an ABI PRISM 7700 real-time PCR system (Applied Biosystems) with the following cycler conditions: an initial activation step for HotStar *Taq* polymerase at 95°C for 15 min and a subsequent 50 cycles at 94°C for 15 s and 60°C for 60 s. Graded numbers of linearized plasmid pDrive_gB_PTHrP_Tdy were used as the template for standard curves. PCR efficiency ranged between 96% and 100%, with correlation coefficients of ≥0.99 in the reported experiments.

(ii) Quantitation of viral DNA in plantar tissue. As inflammatory infiltrates are absent or negligibly present after hematoablative γ irradiation, data for the viral sequence could be normalized to the cellular *pthrp* gene. Plantar tissue, consisting of skin, fat tissue, connective tissue, muscle tissue, vessel walls, cartilage, and bones, was homogenized with a QIAGEN MM300 mixer mill at 30 Hz for two 5-min intervals by use of two 4-mm-diameter steel balls. Of each homogenate, 25-mg portions were used for DNA isolation with a DNeasy tissue kit (catalog no. 69506; QIAGEN) as described previously (65). Viral and cellular genomes were quantitated with SYBR green PCR in an Applied Biosystems 7500 real-time PCR system, using a QuantiTect SYBR green PCR kit (catalog no. 204143; QIAGEN) essentially as described previously (65) except for the following modification of cycler conditions: an initial activation step for 15 min at 95°C was followed by 45 cycles of 15 s at 94°C, 30 s at 62°C, and 45 s at 72°C. After amplification, melting curve analysis of the PCR products was performed by raising the temperature to 95°C, cooling down to 60°C for 60 s, and then raising the temperature again to 95°C with continuous recording of fluorescence to exclude unspecific amplification of primer dimers.

Immunohistochemical detection of infected cells in the liver. (i) Two-color IHC for simultaneous detection of E12E lymphoma cells and of cells infected with mCMV-WT or mutants. Deparaffinized 2-μm sections of liver tissue were stained in a first step for cell surface protein CD45R/B220 (see above) and in a second step for the intranuclear IE1 protein (pp76/89) of mCMV as described in greater detail previously (24). In essence, E12E cells are stained black by using MAb RA3-6B2 and the ABC-peroxidase DAB-nickel method, whereas infected cells are stained red by using the IE1-specific MAb CROMA 101 (kindly provided by S. Jonjic, University of Rijeka, Rijeka, Croatia) and the alkaline phosphatase-antialkaline phosphatase fuchsin method.

(ii) IHC for detection of cells infected with HSV. Deparaffinized 2-μm sections of liver tissue were digested for 15 min at 37°C in EDTA-trypsin solution (10× concentrate, catalog no. L11-003; PAA Laboratories, Pasching, Austria) for epitope retrieval. Endogenous peroxidase was blocked for 35 min at 20°C with methanol-PBS solution (1:1 [vol/vol]) containing 0.5% (vol/vol) hydrogen peroxide. Specific labeling was performed for 30 min at 20°C with a 1:250 dilution of primary antibody in PBS. Purified Ig fractions of rabbit antisera anti-HSV type 1 (HSV-1) and anti-HSV-2 (catalog no. B0114 and B0116, respectively; Dako-Cytomation, Hamburg, Germany) were used as primary antibodies. Biotinylated goat antiserum directed against rabbit IgG (catalog no. B8895; Sigma, Taufkirchen, Germany), diluted 1:500 in Tris-buffered saline, was used as the secondary antibody for 30 min at 20°C. Brown staining was performed with an ABC-peroxidase kit (PK-4000; Vector Laboratories, Burlingame, Calif.) for 30 min at 20°C and with the substrate DAB (catalog no. D5637; Sigma) for 20 min.

In situ detection of apoptotic E12E lymphoma cells. Apoptotic E12E cells were detected by two-color IHC staining of cell surface CD45R/B220 in black and of cytoplasmic active caspase 3 in red. For antigen unmasking (heat-induced epitope retrieval), deparaffinized 2-μm sections of liver tissue were incubated in trisodium citrate-dihydrate buffer (10 mM; pH 6), boiled three times for 2 min in a microwave oven, and subsequently cooled down to room temperature for 45 min. After blocking of endogenous peroxidase (see above), sections were labeled for 1 h at 20°C with the first primary antibody anti-mouse CD45R/B220 [rat IgG2a(κ), clone RA3-6B2, catalog no. 553084; BD-Biosciences, Heidelberg, Germany] diluted 1:250 in PBS. This was followed by an incubation for 30 min at 20°C with the secondary antibody, which was a biotinylated polyclonal goat serum directed against rat Ig (catalog no. 554014; BD Biosciences, Heidelberg, Germany) diluted 1:100 in PBS. Black staining was performed with the ABC-peroxidase kit and DAB as the substrate (see above) with nickel enhancement of color (ammonium nickel sulfate hexahydrate, catalog no. A1827; Sigma). After

washing in PBS for 30 min at 20°C, sections were incubated for 18 h at 20°C with the second primary antibody anti-caspase 3 (affinity-purified polyclonal rabbit IgG, catalog no. AF835; R&D Systems, Wiesbaden, Germany) diluted 1:50 in PBS. Sections were incubated for 30 min at 20°C with a "bridging antibody" goat anti-rabbit IgG (polyclonal goat IgG, catalog no. R5506; Sigma) diluted 1:10 in PBS. Staining was performed for 30 min at 20°C with rabbit alkaline phosphatase-antialkaline phosphatase complex (calf intestinal alkaline phosphatase and rabbit antiserum to alkaline phosphatase, catalog no. A9811; Sigma) diluted 1:10 in PBS and with fuchsin (catalog no. K0624; DakoCytomation) as the chromogenic substrate that yields a red coloration.

RESULTS

Survival benefit from concomitant mCMV infection depends on the initial tumor cell burden. After hematoablative treatment of BALB/c mice, infection with wild-type mCMV, strain Smith (mCMV-WT), leads to lethal multiple-organ CMV disease, whereas hematopoietic reconstitution by BMT restores protective antiviral CD8 T cells that control the infection and thereby prevent infection-associated death (references 2, 54, and 55; for a recent review, see reference 34). Growth of the BALB/c-derived liver-adapted E12E B-cell lymphoma is also lethal after hematoablative treatment of recipients, but in this case, hematopoietic reconstitution has no significant impact on tumor growth and tumor-associated death (24), which indicates a low immunogenicity of E12E. Surprisingly, concomitant infection with mCMV-WT was found to inhibit the growth of the E12E lymphoma and to prolong the median survival time in BMT recipients (24). Thus, in this model, mCMV controls the tumor and reconstitution by BMT controls mCMV.

The original experiments that led to the discovery of this antitumoral link were performed with 10^6 E12E cells, which is a fairly high tumor cell burden not representing a close model for minimal residual disease/leukemia (see the introduction). We therefore tested the effect of mCMV-WT infection on the survival rate of BMT recipients with the tumor cell number being the variable parameter (Fig. 1). As expected, the initial number of administered tumor cells determined the tumor-associated lethality in BMT recipients. Specifically, the median survival time increased from ~6.5 weeks with 10^6 E12E cells (Fig. 1A) to ~9 weeks with 10^5 E12E cells (Fig. 1B) and to ~4 months with 10^4 E12E cells (Fig. 1C), with end point (defined by a 12-month observation period) survival rates of 0%, 8%, and 28%, respectively. A concomitant infection with mCMV-WT increased the median survival time from ~6.5 weeks to ~9.5 weeks in the case of the experiment with 10^6 E12E cells (Fig. 1A), which is in good accordance with previous data (24). The survival benefit was more pronounced at a lower initial tumor cell burden. Specifically, the median survival time increased from ~9 weeks to ~8 months with 10^5 E12E cells (Fig. 1B) and from ~4 months to >1 year with 10^4 E12 cells (Fig. 1C), with end point survival rates of 8% (for 10^6 E12E cells), 12% (for 10^5 E12E cells), and 56% (for 10^5 E12E cells).

Late mortality (at >4 months) in the infected groups was supposed to result from tumor relapse. However, histopathological examination upon autopsy did not reveal any tumor relapse, and there was also no indication for recurrent productive infection being the cause of death (J. Podlech, data not shown). Since the time of mortality was apparently determined by the initial number of tumor cells (compare Fig. 1B with C), we suspect that a preceding tumor burden more generally reduces the life expectancy for reasons yet to be explored.

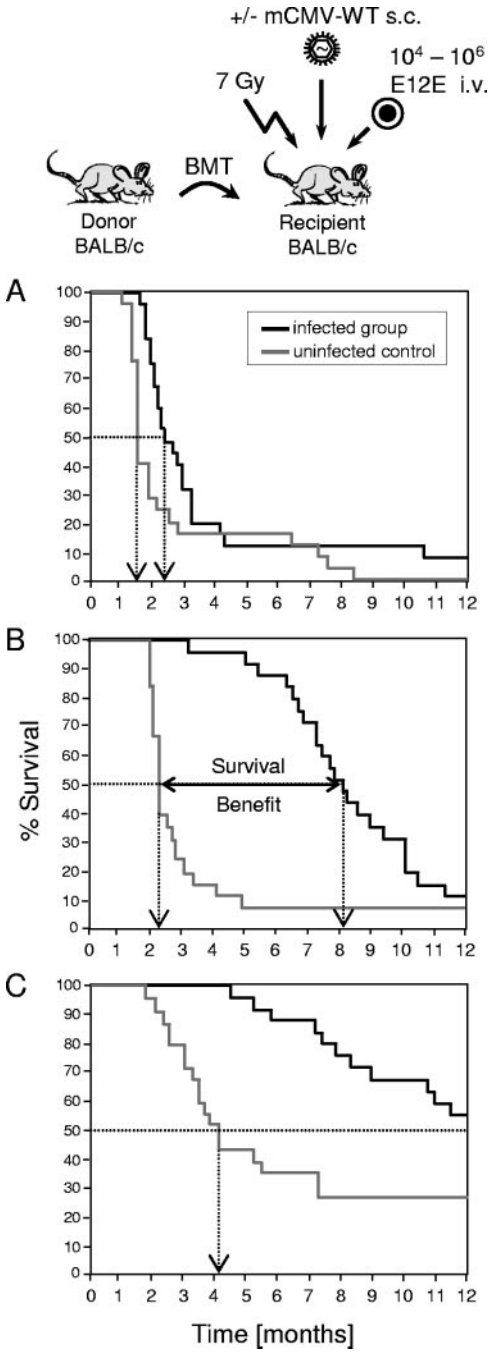

FIG. 1. Effect of the E12E lymphoma cell dose on the median survival time. Syngeneic BMT with BALB/c mice as donors and recipients was performed with 10^7 donor bone marrow cells at 1 day after a 7-Gy hematoablative conditioning of the recipients. Graded doses of E12E cells were given i.v. together with the bone marrow cells, followed by subcutaneous (s.c.) (intraplantar) infection with 10^5 PFU of mCMV-WT. (A) 10^6 E12E cells; (B) 10^5 E12E cells; (C) 10^4 E12E cells. Survival was monitored over a period of 12 months for 25 recipients per group. Shown are Kaplan-Meier plots with black and gray lines representing infected and uninfected groups, respectively. Dotted arrows mark the median survival times.

In conclusion, this set of data has shown that mCMV infection conveys a significant survival benefit in terms of prolonged median survival times, particularly at lower initial tumor cell burdens. This is of potential relevance, because in clinical

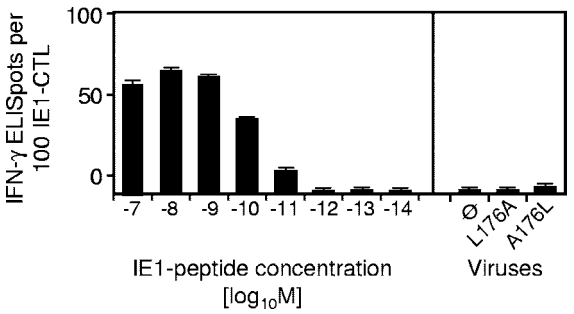

FIG. 2. Presentation of IE1 peptide by E12E cells. IE1 epitope-specific CD8 T cells (IE1-CTL) were used as effector cells in an IFN-γ-based ELISPOT assay to detect a possible presentation of the IE1 peptide on E12E cells that were either loaded exogenously with synthetic IE1 peptide at the indicated peptide concentrations or exposed to viruses mCMV-IE1-L176A and mCMV-IE1-A176L at a dose of 4 PFU/cell. Group ∅, uninfected E12E stimulator cells with no peptide added. The number of responding, spot-forming IE1-CTL was counted for seedings of 400, 200, 100, and 50 IE1-CTL. Black bars indicate the most probable numbers per 100 IE1-CTL as determined by intercept-free linear regression analysis. The error bars indicate the upper 95% confidence limits. *P* values for nonlinearity (null hypothesis) were <0.001 throughout.

BMT, tumor relapse after hematoablative therapy of leukemia typically originates from low numbers of surviving tumor cells (12, 16).

E12E lymphoma cells are not a target for IE1-specific CD8 T cells. Infection of BMT recipients with mCMV-WT leads to the reconstitution of a vigorous antiviral CD8 T-cell response that controls the infection and prevents CMV disease (see reference 36; also reviewed in reference 34). It was therefore an immediate idea that E12E cells, although not permissive for productive infection, might present viral peptides resulting from limited gene expression, preferably of IE genes, and become a target for antiviral CTL. As shown in our previous report (24), a CTL line specific for the L^d-restricted, immunodominant IE-phase peptide IE1 of mCMV (58, 59) prevents infection-associated death upon adoptive transfer into recipients of low-dose BMT that otherwise would have developed CMV disease. In absence of infection, transfer of IE1-CTL did not impact on the E12E lymphoma (24), which indicates that IE1-CTL do not cross-react with a putative nonviral epitope constitutively presented by E12E. However, since resolution of the infection by IE1-CTL did not abolish the antitumoral effect, recognition of E12E cells presenting the IE1 peptide remained a possible mechanism of tumor control. Although immunofluorescence analysis did not reveal the expression of intranuclear IE1 (pp76/89) protein by E12E cells incubated with mCMV-WT at a dose of 4 PFU per cell (K. C. Erlach, unpublished results), limited expression of IE genes and trace presentation of the IE1 peptide was not yet formally excluded. We have therefore directly addressed this possibility. As shown in Fig. 2, E12E cells are capable of presenting exogenously loaded synthetic IE1 peptide for recognition by IE1-CTL at concentrations of $>10^{-12}$ M, but they did not present naturally processed IE1 peptide after exposure to infectious mCMV-WT-like revertant virus mCMV-IE1-A176L encoding the antigenic IE1 peptide. Furthermore, the antitumoral effect was also elicited by the corresponding mutant virus mCMV-IE1-L176A, a virus in which the antigenicity of the IE1 peptide is wiped out by mutation of the C-terminal MHC anchor residue Leu to Ala (data not shown). This clearly implies that recognition of the IE1 epitope is not involved in E12E growth control. At this stage of experimentation, it remained a possibility that a strong antiviral immune response after BMT not only controls the infection but also exerts a bystander effect, for instance through induction of cytokines, that might enhance a graft-versus-leukemia reactivity.

Control of B- and T-cell lymphomas in the absence of BMT. Our previous finding that infection with mCMV-WT inhibits the E12E lymphoma after a 7-Gy hematoablative treatment also in the absence of bone marrow reconstitution by BMT (24) argues against a primarily immunological mechanism. By definition, a graft-versus-leukemia reactivity cannot occur in the absence of a hematopoietic graft, and it is also evident that a bystander activation cannot take place in the absence of an antiviral immune response. Figure 3A recapitulates and experimentally reproduces the previous key finding of E12E control by mCMV-WT in the setting of lethal CMV disease after hematoablative treatment with no immune cell reconstitution (24): whereas on day 12 after i.v. administration of 10^6 E12E cells ~10% of the liver section area were occupied by lymphoma, tumor burden was reduced to ~1% area coverage by concomitant intraplantar infection with mCMV-WT. Computer-assisted imaging and morphometrical analysis indicated a lower number of tumor colonies per area as well as a smaller average size of the tumor colonies.

It has been frequently asked whether this antitumoral effect of mCMV-WT is limited to the liver-adapted and almost completely liver-restricted B-cell lymphoma, clone E12E, or also applies to other lymphomas and other organ sites of tumor cell metastasis. It should be recalled that the antitumoral effect of mCMV-WT was originally discovered for the parental B-cell lymphoma A20, a highly invasive lymphoma that colonizes the intestine, spleen, liver, lungs, and bone marrow of immunocompromised recipients (23). The A20 tumor model was subsequently dismissed because the tumor also infiltrated retroperitoneal tissue, paravertebral musculature, and the spinal cord, resulting in an ethically intolerable paralysis, and because tumor growth was difficult to quantitate histologically. Nonetheless, the A20 model has contributed the important information that the antitumoral effect of mCMV-WT is not tumor cell clone specific or restricted to liver metastases. As shown in Fig. 3B, the effect is also not restricted to tumors of the B-cell lineage. Specifically, mCMV-WT diminished the growth of ESb-derived T-cell lymphomas, namely, the attenuated ESb variant ESb-MP (6) and the highly aggressive, hepatotropic variant ESb-L-CI (39, 44). Work on nonlymphoma tumor models is in progress.

Infection dose dependence and virus-type specificity of the antitumoral effect. The virus dose and infectivity were found to be decisive for triggering E12E lymphoma control. Specifically, 10 PFU of mCMV-WT had no significant effect (up to four tumor size classes were seen, as for the control), 10^3 PFU reduced the number and average size of tumor colonies (size classes 1 and 2 only), and 10^5 PFU largely controlled the lymphoma with only small (size class 1 only) and few colonies remaining (Fig. 4A). Incidentally, hCMV strain Towne failed in accordance with the species specificity of the betaherpesvi-

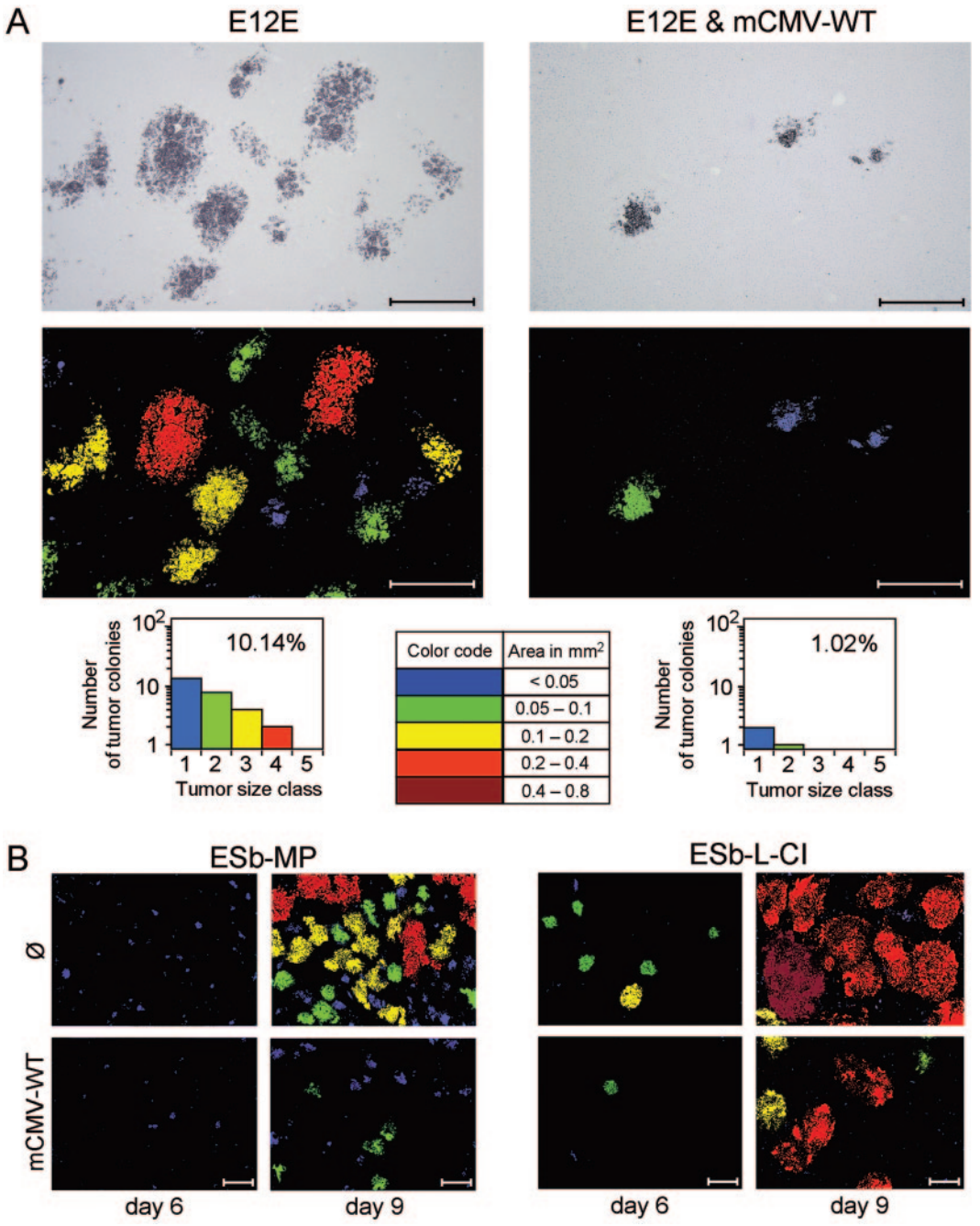

FIG. 3. Lymphoma imaging and computer-assisted quantitation. BALB/c mice were treated like BMT recipients (Fig. 1), except that no BMT was performed. (A) Effect of mCMV-WT on the E12E lymphoma. E12E cells (10^6) were administered i.v. at ~1 h before infection. (Left column) No infection; (right column), subcutaneous (s.c.) (intraplantar) infection with 10^5 PFU of mCMV-WT. Lymphoma colonies in the liver were detected on day 12 by IHC specific for the cell surface antigen CD45R (black staining with light hematoxylin counterstaining). Bar markers represent 500 μm and the displayed tissue section area measures ~4 mm^2. Five tumor size classes were defined as indicated, and the colonies were color coded correspondingly in blue, green, yellow, bright red, and Bordeaux red with log 2-increasing size. Quantification was performed for the displayed tissue section area by counting the number of tumor colonies for each tumor size class, depicted as a "tumor size-frequency diagram." The percentages of liver tissue area covered by tumor are indicated in the tumor size-frequency diagrams. (B) Effect of mCMV-WT on T-cell lymphomas. Shown are the color-coded CD45R IHC images of liver tissue sections on days 6 and 9 after i.v. tumor cell administration and intraplantar infection with 10^5 PFU of mCMV-WT. ∅, uninfected control group. (Left panel) 10^5 cells of the attenuated lymphoma ESb-MP; (right panel) 10^3 cells of the highly aggressive lymphoma ESb-L-CI. Bar markers represent 500 μm.

ruses. It should be recalled that previous work has already shown that virion proteins of 254-nm UV light-inactivated mCMV-WT^{UV} do not control the E12E lymphoma after intraplantar administration of a dose equivalent to 10^6 PFU (24).

It was an obvious question whether productive intraplantar infection with any other virus or whether a "viral disease syndrome" as such could inhibit the growth of a lymphoma by unspecific means such as hyperthermia, hypoxemia, withdrawal

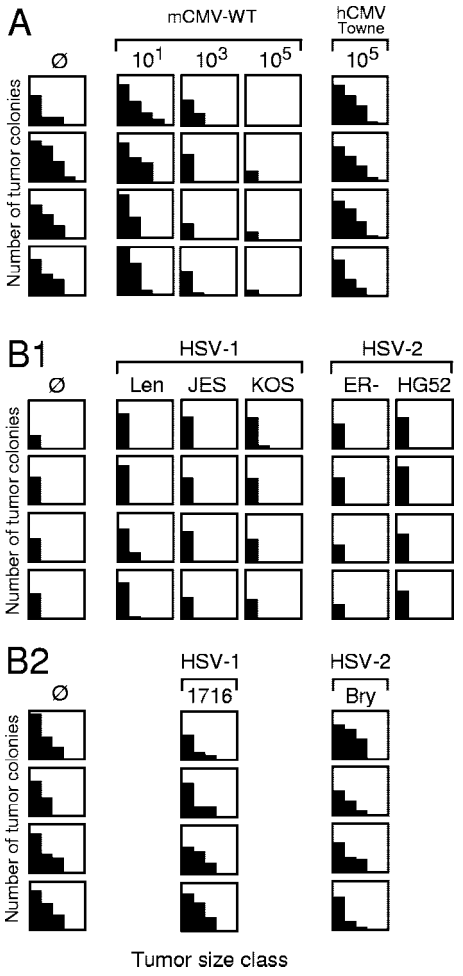

FIG. 4. Virus dose dependence and specificity of E12E growth inhibition. For the experimental protocol and the principle of lymphoma quantification, see the legend for Fig. 3A; here, however, tumor colonies were counted in a more representative tissue section area of 100 mm^2. Throughout, 10^6 E12E cells were administered i.v., and infections were performed subcutaneously (intraplantar) with the indicated viruses and virus doses. Groups ∅, no infection. (A) Virus dose dependence and betaherpesvirus host species specificity. Infection doses in PFU are indicated. IHC for lymphoma quantification in liver tissue sections was performed on day 12. (B1) Infection with 10^4 PFU of the indicated virulent strains of the alphaherpesviruses HSV-1 and HSV-2. Because of high lethality, the readout was on day 7. Accordingly, only one tumor size class is occupied in the tumor size-frequency diagrams. (B2) Infection with 10^5 PFU of the indicated attenuated strains of HSV-1 and HSV-2. The readout was on day 12. Each tumor size-frequency diagram represents the result for an individual mouse, with four mice tested per experimental group.

of nutrients and growth factors, or cytokine burst and endothelial injury. For a rational comparison, we have chosen the related herpesviruses HSV-1 and HSV-2. In BALB/c mice immunocompromised by the 7-Gy hematoablative treatment, strains KOS (7), JES (42), and Len (25) of HSV-1 as well as ER^- (56) and HG52 (68) of HSV-2 replicate vigorously at the plantar site of infection, cause the typical herpetic lesions of the skin, and lead to lethal systemic disease. Despite local replication at the inoculation site and lethal disease, none of these five HSV strains had any impact on the growth of the E12E lymphoma in the liver (Fig. 4B1). Because of the high lethality, the tumor sizes in this experiment had to be assessed as soon as day 7. For a closer kinetic comparison with mCMV-WT and assessment of tumor sizes on day 12, we also used the less pathogenic strains 1716 of HSV-1 deficient in the neurovirulence determinant ICP34.5 (47) and Bry of HSV-2 deficient in the thymidine kinase (26). Again, there was no effect on the growth of the E12E lymphoma in the liver (Fig. 4B2). It is worth noting that we refrained from testing the gammaherpesvirus MHV-68, because its tropism for B cells may exert an effect on the B-cell lymphoma E12E that is unrelated to the antitumoral mechanism under investigation.

An objection might be raised against comparison with HSV strains because of their lethality due to neuroinvasiveness and suspected lack of hematogenic spread. However, as shown in Fig. 5 for the example of HSV-1 strain JES (likewise for HSV-1 strain KOS and HSV-2 strain ER^- [not shown]), intraplantar HSV disseminates to the liver and replicates in hepatocytes under the immunosuppressive conditions used for the tumor experiments. Serial sections of liver tissue reveal quite a pronounced perivascular HSV infection (Fig. 5A1 and A2) and a lack of infection of the neighboring E12E tumor noduli (Fig. 5B1 and B2). In fact, sites of infection and sites of tumor growth appear to be mutually exclusive. Thus, although HSV disseminates to the liver, it does not inhibit the growth of the lymphoma.

In conclusion, the antitumoral effect is specific for mCMV and is virus dose dependent.

Role of local intraplantar virus replication and of viremic dissemination. To assess the requirement for viral replication and dissemination in exerting the antitumoral effect, we used real-time quantitative PCR to quantitate viral genomes at the site of inoculation, that is, in footpad tissue, as well as in the blood in a kinetics experiment (Fig. 6). Infection with mCMV-WT provided a positive control for replication and dissemination of infectious virus, whereas 254-nm UV light-inactivated mCMV-WT^{UV} allowed us to track the fate of inoculum genomes. As UV light not only has effects on DNA but also induces free radicals and might alter virion proteins photochemically, mutant virus mCMV-ΔMIEenh that lacks the enhancer as the major genetic *cis*-control element of IE transactivator gene expression was employed as a virus made genetically deficient for in vivo replication (29). Finally, mutant mCMV-ΔM36 lacking the antiapoptotic *M36* gene essential for replication in macrophages (48) was used as a virus that is deficient in viremic dissemination (18). In accordance with the known properties of the chosen viruses, only mCMV-WT and mCMV-ΔM36 were found to significantly replicate in footpad tissue (Fig. 6A), whereas only mCMV-WT genomes were detected in the blood at later times (Fig. 6B).

The productive infection of liver tissue is the most dependable and most sensitive marker for virus dissemination from the footpad to the liver. We have therefore used two-color IHC to directly relate infection of the liver to tumor growth in the liver (Fig. 7). As shown in Fig. 7A1, infected liver cells, which are predominantly hepatocytes, can first be detected (detection limit, ≥1 cell per 10 mm^2) on day 3.3 (95% confidence interval, day 2.3 to day 4.5) after intraplantar infection of immunocompromised (7-Gy-irradiated) BALB/c mice with 10^5 PFU of mCMV-WT. After the virus had reached the liver, the number

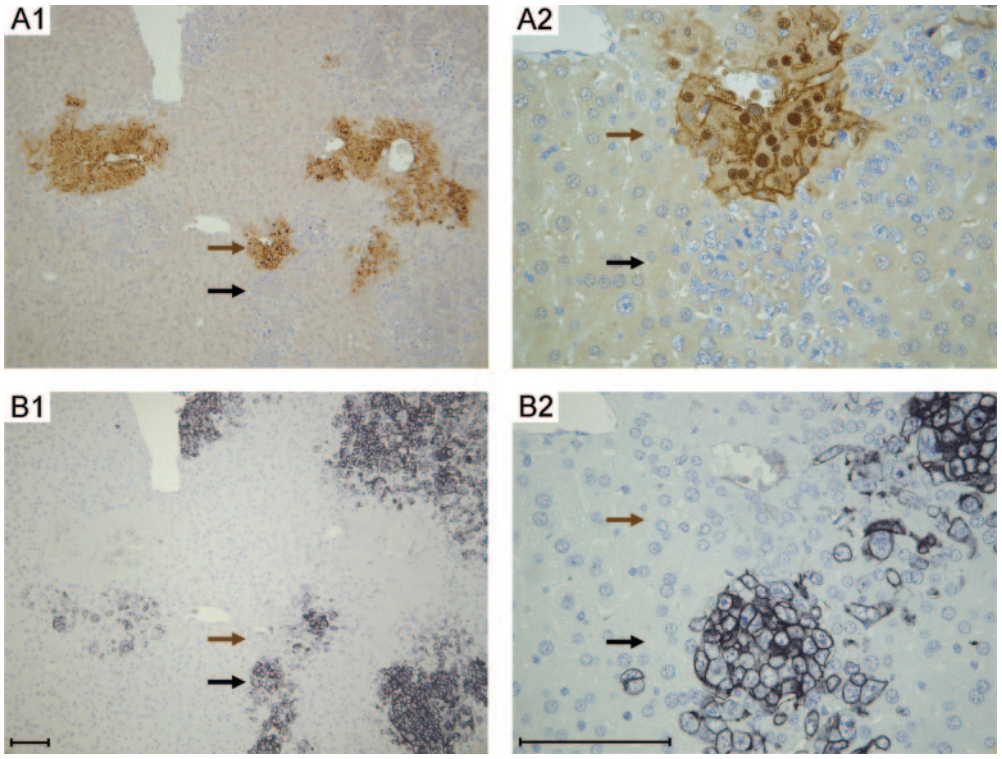

FIG. 5. Dissemination of HSV-1 strain JES to the liver. Intraplantar infection of the immunocompromised recipients (protocol as for Fig. 3A) was performed with 10^3 PFU of HSV-1 strain JES. On day 11, a prefinal stage of viral disease, infected liver cells and E12E lymphoma cells were detected in serial 2-μm liver tissue sections. (A) Infection of perivascular hepatocytes detected with anti-HSV polyclonal immunoglobulin. Brown DAB staining with hematoxylin counterstaining. A1, overview; A2, detail. (B) Neighboring section with E12E lymphoma colonies detected with MAb directed against cell surface antigen CD45R. Black DAB-nickel staining with hematoxylin counterstaining. B1, overview; B2, detail. Bar markers represent 100 μm. Brown and black arrows highlight the location of foci of infection and of lymphoma colonies, respectively. Note that areas with intense hematoxylin staining correspond to tumor localization.

of infected cells increased in a log-linear function by a factor of 1,000 to ~10^3 per 10 mm^2 on day 10 (Fig. 7A1). The corresponding two-color IHC image on day 10 shows massive tissue infection and viral histopathology with numerous infected hepatocytes (Fig. 7A2 and A3; red staining of intranuclear IE1 protein pp76/89) but no tumor cells.

As expected, inactivated virus mCMV-WT^{UV} failed to infect the liver and also failed to control the tumor (Fig. 7B). The enhancer-deficient mutant mCMV-ΔMIEenh behaved like mCMV-WT^{UV} in that it failed to infect the liver and to control the tumor (Fig. 7C). At this stage of experimentation, one is easily misled to draw the conclusion that tumor control in the liver correlates with virus dissemination to and infection of the liver. The decisive information came from the dissemination-deficient mutant mCMV-ΔM36. This virus failed to infect the liver and did not cause generalized CMV disease but nevertheless controlled the E12E lymphoma (Fig. 7D). This is the exact opposite of the situation described above for HSV-1 strain JES, which infected the liver but nevertheless failed to control the E12E lymphoma (recall Fig. 5). In conclusion, control of lymphoma growth in the liver is specifically triggered by a distant productive mCMV infection without a need for viremic dissemination and infection of the liver.

Virion proteins do not affect proliferation in cell culture and tissue homing of E12E lymphoma cells. As discussed above, E12E cells are not permissive for productive infection with mCMV-WT and do not even express IE proteins. However, it is well established that mere virion binding and entry in absence of viral gene expression can by themselves induce global changes in cellular transcription, that of interferon-responsive genes in particular (for a recent review, see reference 10), and this could possibly affect the tumorigenicity of E12E cells. One parameter that determines tumorigenicity is the doubling time. In accordance with previous data (24), Fig. 8A shows that mCMV-WT^{UV} and mCMV-WT have no significant influence on the doubling time of E12E cells in cell culture (~32 h), a conclusion that is based on largely overlapping 95% confidence intervals for the doubling time in a log-linear regression analysis.

Another parameter that determines tumorigenicity is the tumor cells' capacity to leave the circulation by migrating through the endothelium for homing in tissue. Masking of receptors on the tumor cell surface by the binding of virion proteins as well as the modulation of cell surface molecule expression, for instance, integrin expression, might inhibit the extravasation of the lymphoma cells. We have not specifically looked at changes in gene expression or cell surface molecules induced in E12E cells by virion binding and the entry process but instead have chosen a straightforward functional approach. As shown in Fig. 8B, pretreatment of E12E cells with high doses (an equivalent of 4 PFU per cell) of mCMV-WT^{UV} or mCMV-ΔMIEenh before their intravenous infusion had no

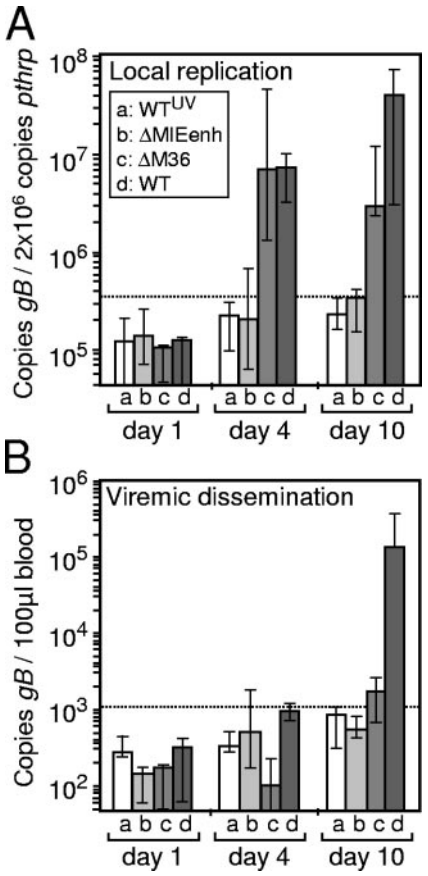

FIG. 6. Local virus replication and viremic dissemination. For the protocol, see legend for Fig. 3A. (A) Virus replication at the intraplantar site of inoculation. The increase in viral copy numbers was monitored by real-time quantitative PCR specific for the *M55*/*gB* gene and normalized to the copy number of the autosomal cellular gene *pthrp*. (B) Viral genomes present in peripheral blood. The increase in viral copy numbers was monitored as described above, except that data were normalized to a defined volume to take account of increasing leukocytopenia as a result of the 7-Gy γ irradiation. Virus doses were 10^5 PFU or PFU equivalents throughout. (a) WT^{UV}, 254-nm UV light-inactivated mCMV-WT; (b) ΔMIEenh, enhancerless mutant mCMV-ΔMIEenh; (c) ΔM36, mutant virus mCMV-ΔM36 lacking the anti-apoptotic gene *M36*; (d) WT, mCMV-WT. Bars represent median values of triplicates with the error bars representing the ranges. The dotted lines indicate the significance limit of replication as defined by the highest value detected for replication-incompetent mCMV-WT^{UV} representing inactivated inoculum genomes.

influence on the growth of the E12E lymphoma in the liver. Thus, whatever changes virion proteins may induce in E12E cells, these changes are apparently not relevant for tumorigenicity. In conclusion, inhibition of the E12E lymphoma does not result from a direct physical interaction between E12E cells and virions.

Distant infection induces transient apoptosis in young E12E lymphoma colonies in the liver. Up to this point, inhibition of the E12E lymphoma in the liver has been assessed by comparing the tumor burden, as defined by number and size of tumor noduli (Fig. 3), at a relatively advanced stage. It is inherent to an exponential growth function that tiny differences at early stages develop into huge differences at later stages. Thus, for instance, small differences in the growth rate could account for clinically significant differences in late tumor burden. Likewise, small differences in the number of tumor cells that enter exponential growth after successful extravasation and homing in the liver can also lead to significant differences at later stages. Based on this mathematical understanding, we developed an assay to experimentally determine the in vivo growth rate of the lymphoma cells, reflected by their doubling time in the liver, as well as the transmigration rate, reflected by the initial number of lymphoma cells present in a defined area of liver tissue (Fig. 9A and B). Figure 9A shows the raw data on E12E lymphoma growth in a semilogarithmic plot of counted tumor cell numbers per unit area (log; ordinate) as a function of time (linear; abscissa), and Fig. 9B shows the corresponding calculated log-linear regression lines. From slope a of the regression line, the doubling time can be calculated by the equation $DT = \log 2/a$, and extrapolation of the regression line to time zero reveals the transmigration rate as the ordinate intercept. An important boundary condition for the calculation is that tumor cells enter the liver parenchyma by transmigration at the sinusoidal endothelium within the first hours and that there is no further influx during the subsequent days. It has long been known that tumor cells rapidly die in the circulation due to biomechanical trauma and that extravasation is therefore the critical step in tumor cell survival and metastasis (69, 70). We have used the *lacZ* reporter gene present in transfected clone E12E (24) to measure the physical half-life of E12E cells (cells physically present but not necessarily still viable) in the circulation by quantitative PCR and found a value of ~50 min (95% confidence interval, 47 to 54 min). Accordingly, in a conservative estimate, an intravenous inoculum of 10^6 tumor cells drops to <100 circulating tumor cells within 12 h. Probably, as suggested by the literature (69, 70), the half-life of viable tumor cells is even significantly shorter. As the liver-adapted E12E lymphoma metastasizes almost exclusively to the liver, there is also no late immigration into the liver from extrahepatic sites. Thus, in good approximation, the boundary condition for the calculation is fulfilled.

Growth kinetics. (i) E12E lymphoma growth kinetics in the absence of infection. During an observation period of 7 days, the E12E lymphoma cells were found to grow exponentially with a doubling time of 26.4 h (95% confidence interval, 24.3 to 28.9 h). The log-linear increase in cell numbers indicates optimal conditions for unrestricted growth in the liver. Notably, within the 95% confidence intervals, the doubling times were basically the same in vivo and in cell culture (recall Fig. 8A). The number of transmigrated E12E cells was determined as being 15 (95% confidence interval, 12 to 20 cells) in the unit area, which was 50 mm^2 in the reported experiments.

(ii) E12E lymphoma growth kinetics in the presence of infection. Since we had predicted that infection reduces either the transmigration rate or the doubling time of the E12E cells or possibly both, the result of the experiment came as a true surprise and was in fact unpredictable. First, the transmigration rate of 11 cells (95% confidence interval, 5 to 26 cells) was essentially the same as in the uninfected group. Second, the transmigrated cells proliferated within the liver with unaffected doubling time until day 2, which corresponds to young tumor cell colonies in the four-cell stage. Both findings imply that the tumor cells were not affected by the infection during their floating in the circulation, transmigration at interendothelial

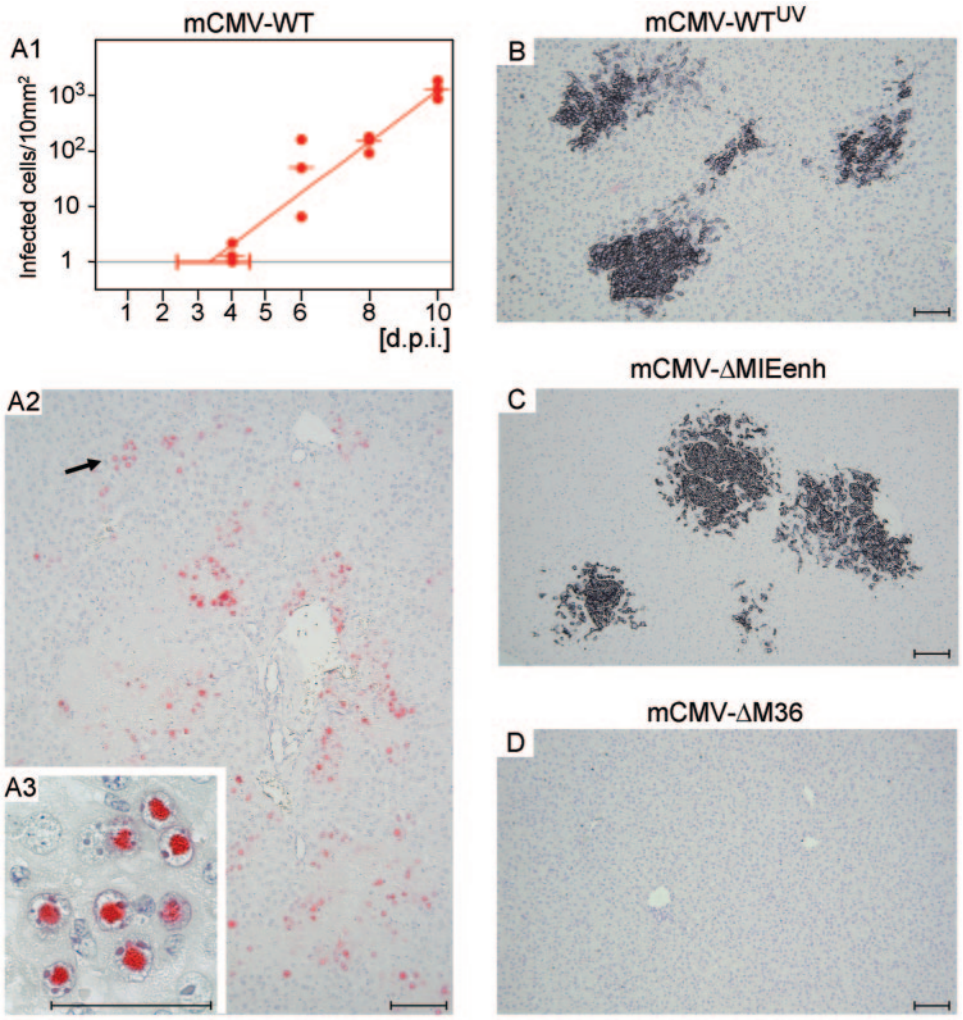

FIG. 7. Lymphoma growth and virus replication in the liver. The experiment was the same as that shown in Fig. 6, with 10^6 E12E lymphoma cells administered i.v. and intraplantar infection/inoculation of 7-Gy-γ-irradiated BALB/c mice with the viruses indicated. Shown is two-color IHC analysis for the simultaneous detection of E12E cells (black staining of CD45R) and of infected hepatocytes (red staining of intranuclear IE1 protein pp76/89) in liver tissue sections. Counterstaining was performed with hematoxylin. (A1) Kinetics of mCMV-WT infection of the liver. The number of infected hepatocytes per 10 mm^2 (n_t) was determined for three individual recipients per time point and is indicated by dots with the median values marked. Log-linear regression analysis reveals the time point of first detectability of liver infection from the point of intersection between the calculated regression line, $\log n_t = at + \log n_0$, and the line $\log n_t = 0$ (1 infected cell per detection area; dotted line). The horizontal bar represents the 95% confidence interval of the time point of first detectability. d.p.i., day postinfection. (A2). Histological image of liver infection on day 10. The bar marker represents 100 μm. The arrow points to a group of infected hepatocytes that is resolved to greater detail in A3. (A3) Group of infected hepatocytes identified by intranuclear inclusion bodies containing IE1 protein pp76/89. The bar marker represents 50 μm. (B through D) Infection/inoculation with the viruses indicated, and two-color IHC performed on day 12. Bar markers represent 100 μm.

junctions, early tissue homing, and initial proliferation. Between days 2 and 5, however, the number of tumor cells declined; this decline, notably, was also in a log-linear function with a "negative doubling time," or half-life of ~29 h, to a level below the initial transmigration rate. Strikingly, after this period of remission, remaining tumor cells entered a relapse phase of exponential growth with a doubling time that was essentially the same as that in the uninfected group. This indicates that the surviving tumor cells were not impaired in their proliferative potential by the events that had led to the transient remission. It is important to note that tumor remission took place at a time when liver infection was at its very beginning, whereas tumor relapse occurred at a time of—but in spite of—full-blown liver infection (recall Fig. 7A1). This makes it unequivocally clear that neither an infection of the tumor cells nor a destruction of the stromal "homing bed" of tumor colonies by histopathological, cytolytic tissue infection is responsible for the antitumoral effect.

Unless we assume that tumor cells leave the liver in the period of remission, for which there is no rationale or evidence whatsoever, cell death is the only explanation for a decline in absolute cell numbers. We have therefore performed a two-color IHC analysis to detect and quantitate dying tumor cells in the period of tumor remission (Fig. 9C and D). Coexpression of active caspase 3 and the cell surface marker CD45R identified tumor cells in apoptosis (Fig. 9C). Absence of active

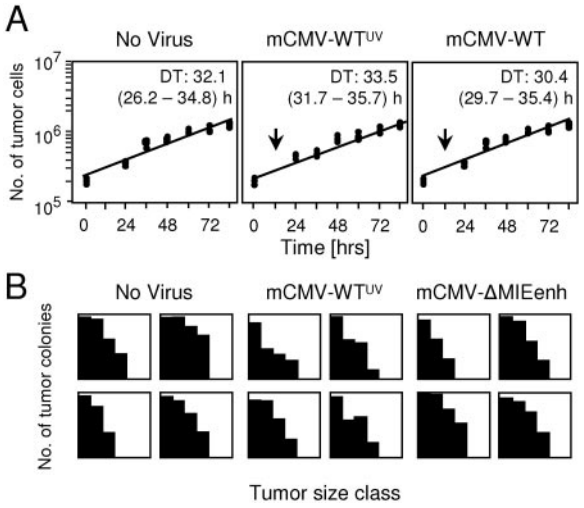

FIG. 8. Effect of virion attachment/entry on E12E growth in cell culture and on in vivo tumorigenesis. (A) Kinetics of tumor growth in cell culture. E12E cells were seeded in triplicate with a starting cell number of 2×10^5 cells per ml of a 2-ml culture. At 12 h after seeding (arrows), mCMV-WT^{UV} or mCMV-WT was added in a dose equivalent to 4 PFU per cell. Tumor cell numbers were determined from aliquots taken every 12 h and are expressed as tumor cells per ml. Log-linear regression analysis was performed to determine the DT (95% confidence interval of DT). (B) In vivo tumorigenesis. E12E cells were preincubated with mCMV-WT^{UV} or mCMV-ΔMIEenh for 3 h at 37°C at doses equivalent to 4 PFU per cell, and tumor burden in the liver (size-frequency diagrams for 100 mm^2) of four individual mice per group was assessed on day 12 after i.v. transfer of 10^6 pretreated E12E cells.

caspase 3 in the surrounding hepatocytes suggests that the apoptosis-triggering event targeted the tumor cells selectively. Quantitation of apoptotic tumor cells in the kinetics experiment revealed a peak of apoptosis, in absolute and relative terms, on days 3 and 4 (Fig. 9D), coincident with the period of tumor remission (Fig. 9B). Specifically, ~50% of the tumor cells were detected in the state of apoptosis; however, the rate of apoptosis is even higher, considering the fact that tumor cells already disintegrated into apoptotic bodies/vesicles escape detection by IHC.

In conclusion, the effector mechanism of the antitumoral effect of mCMV is a transient "apoptotic crisis" induced in developing tumor cell colonies.

Apoptosis reduces the number and size of developing young tumor colonies. So far, we have looked only at changes in the overall tumor cell numbers. To retrieve the full information contained in the IHC analysis, it is also instructive to view the events on the level of tumor cell colonies. It is an evident topological problem that the absolute number of cells in a three-dimensional tumor cell colony cannot be determined from a two-dimensional tissue section, which necessarily underestimates the number and represents a minimal estimate. Nonetheless, provided that a high number of colonies is included in the analysis, the size-frequency distribution (number of colonies plotted against the number of tumor cells per colony) from two-dimensional sections is a representative deduction from the three-dimensional tumor colonies. Figure 10 shows such an analysis of 50 colonies in the infected group and 50 colonies in the uninfected control group for day 5, the transition point from transient tumor remission to relapse in the infected group.

If there existed two distinct types of tumor cell colonies, one type resistant to apoptosis and the other type susceptible to apoptosis, one would predict a reduced total number of colonies due to the extinction of apoptosis-susceptible colonies but an unaltered size-frequency distribution among the apoptosis-resistant, surviving colonies. As it becomes obvious from the distributions compared in Fig. 10, this model is not supported by the data. Rather, the altered size-frequency distribution in the infected group indicates that survival and apoptosis coexisted in individual colonies.

Several interesting messages are revealed by this distribution analysis. (i) Since in the infected group a 20-fold-larger area had to be counted for collecting 50 tumor colonies (1,000 mm^2 versus 50 mm^2), infection apparently has reduced the total number of colonies by a factor of 20; this implies an extinction of most colonies during the apoptotic crisis. (ii) On average, surviving tumor colonies in the infected group were smaller than were colonies at the same time in the uninfected group (144 versus 394 cells per 50 colonies in two-dimensional sections); this implies that a tumor cell colony can be comprised of individually susceptible and resistant cells. (iii) There existed colonies in the infected group that clearly consisted of more than one cell; this implies that tumor relapse in the infected group often starts out from groups of surviving cells rather than from single, apoptosis-resistant tumor cell variants. It is instructive to note that this finding also refutes the idea that tumor relapse in the liver beyond day 5 could originate from single cells repopulating the liver from the circulation. (iv) Transmigration of single tumor cells and 2 days of growth with a DT of ~1 day predicts a four-cell stage of tumor colonies on day 2. This was also supported by an IHC distribution analysis performed on day 2 (data not shown). Since on day 5 some colonies in the infected group clearly consisted of more than four cells (at least 9 colonies out of 50 [Fig. 10, top panel]), tumor cells must have proliferated during the apoptotic crisis between day 2 and day 5. Thus, the overall decline in cell numbers in the transient remission phase has to be interpreted as a net effect of a rate of apoptosis exceeding the rate of proliferation.

Surviving tumor cells are not genetically determined, apoptosis-resistant variants. The most puzzling aspect of the apoptotic crisis was that some of the tumor cells apparently escaped without any impairment of their in vivo proliferative potential. Although E12E is a clone by origin (24), it was an immediate idea that the apoptosis-triggering event may have selected apoptosis-resistant somatic variants. To test this possibility in a serial tumor cell transfer approach, cells of macroscopically visible "relapse tumor" noduli were isolated 7 weeks after infection of BMT recipients, expanded in short-term cell culture, and transferred into infected and noninfected indicator recipients (Fig. 11A). The result was unequivocal in that it showed a susceptibility of the relapsed tumor cells to the virus-induced apoptotic crisis (Fig. 11B). Thus, tumor cells that escaped the apoptotic crisis were not genetically resistant to apoptosis.

Programmed acquisition of reversible resistance to virus-induced apoptosis by young tumor colonies. Absence of apoptotic tumor cells on day 5 (Fig. 9D) and subsequent tumor

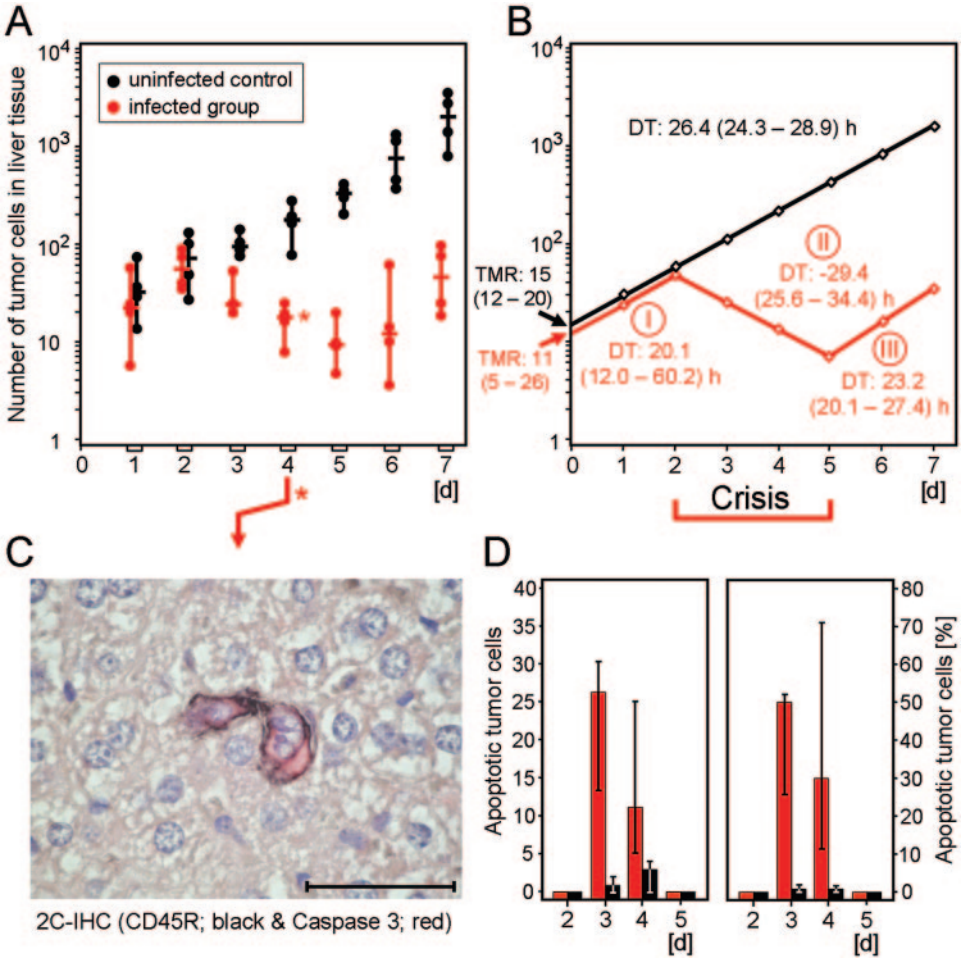

FIG. 9. Apoptotic crisis of E12E lymphoma cells in the liver. (A) Early kinetics of tumor growth in the liver: raw data. For the protocol, see the legend to Fig. 3A. The number of tumor cells was determined by counting of IHC-stained CD45R$^+$ cells in representative 50-mm^2 areas of liver tissue sections. Dots represent data from four individual recipients per time point and group (red symbol, infected with mCMV-WT; black symbol, uninfected) with the median values and ranges indicated by horizontal and vertical bars, respectively. The asterisk marks the individual recipient for which liver histology is shown in panel C. (B) Early kinetics of tumor growth in the liver: results of log-linear regression analysis of the raw data shown in panel A. The plot highlights the monophasic tumor growth in the uninfected group and the triphasic (phases I, II, and III) tumor development in the infected group. DT (95% confidence interval of DT) and transmigration rate (TMR) (95% confidence interval of TMR) are shown. (C) Documentation of tumor-selective apoptosis in the phase of tumor remission (phase II; day 4). For the individual recipient marked by an asterisk in panel A, apoptotic tumor cells are shown in a liver tissue section by two-color IHC with black staining of cell-surface CD45R and red staining of intracellular active caspase 3. The bar marker represents 50 μm. (D) Kinetics of E12E apoptosis. Apoptotic tumor cells (active caspase 3-expressing CD45R$^+$ cells) were counted for representative 50-mm^2 areas of liver tissue sections from four individual recipients per time point and group (red bars, recipients infected with mCMV-WT; black bars, uninfected recipients). (Left panel) Absolute number of apoptotic tumor cells. (Right panel) Percentage of apoptotic tumor cells among all CD45R$^+$ tumor cells. Bars represent the median values and error bars show the range. d, day.

relapse could indicate an acquisition of reversible resistance of the tumor cells against the apoptotic signal. This could be a programmed event regularly associated with the development of young tumor cell colonies after tumor cell homing in tissue. Alternatively, the apoptotic signal itself may be transient, coming like a wave on days 3 and 4 and vanishing by day 5.

In a first approach to decide between these two possible explanations, we asked whether tumor cells also acquire resistance to the apoptotic signal during a phase of growth in the absence of infection and thus in the absence of a selective force. Specifically, susceptibility of tumor cell colonies was investigated in a kinetics experiment (Fig. 12A). E12E cells were administered intravenously on day 0, and intraplantar infection with mCMV-WT was performed at intervals to give the tumor cells a start of 1, 2, 3, 4, or 5 days (Fig. 12A1). Susceptibility to the antitumoral effect was significant until day 2, began to vanish on day 3, and was lost from day 4 onward (Fig. 12A2). For correct interpretation, one has to consider the 2 days' delay in the execution of the effect (recall Fig. 9), so that tumor cell colonies had acquired complete resistance on day 6 corresponding to a 64-cell stage. Notably, this is in fair agreement with the time of relapse observed in the group that was infected on day 0 (recall Fig. 9). It is important to note that the time span between γ irradiation and infection was found to have no influence on the viral triggering of the antitumoral effect, except that γ irradiation should precede infection by ~1 day to allow virus replication (data not shown).

The complementary approach was to give the infection a

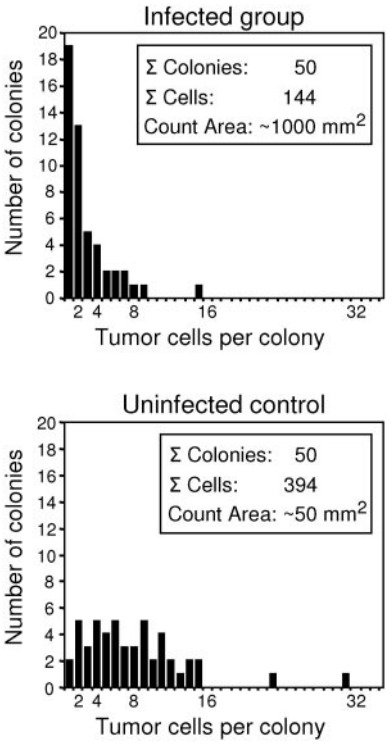

FIG. 10. Tumor colony size distribution at the phase II-to-phase III transition point. For the experiment shown in Fig. 9, the CD45R-IHC data from day 5, the transition point from transient remission to relapse, were evaluated to reveal the numbers of E12E cells in surviving lymphoma colonies. Size (cell number)-frequency plots for the infected group (top) and for the uninfected control group (bottom) are normalized to 50 colonies per group present in ~1,000-mm^2 and ~50-mm^2 areas of liver tissue sections, respectively. This indicates an ~20-fold difference in the total number of lymphoma colonies and an ~50-fold difference in the total number of lymphoma cells. Note that the abscissa has to be interpreted as $\geq n$ tumor cells per colony.

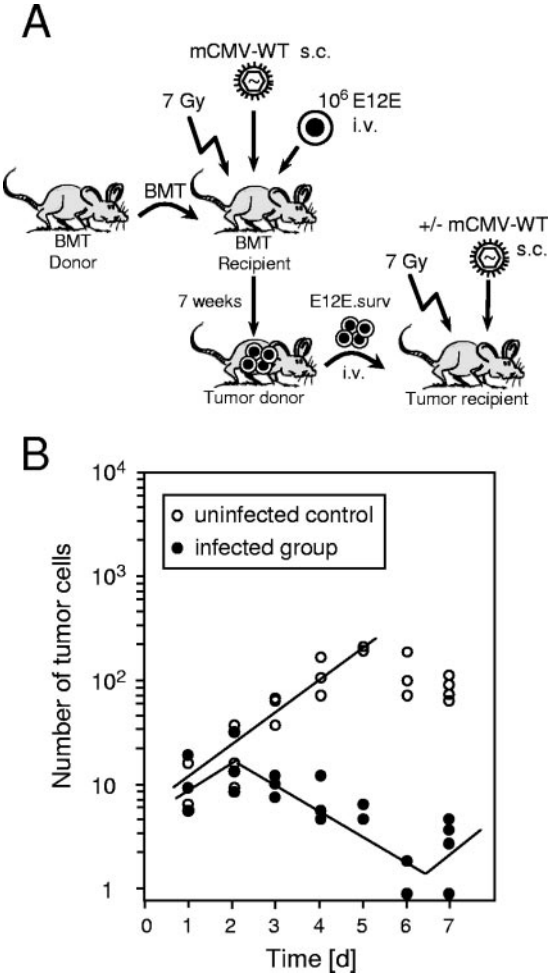

FIG. 11. Serial transfer of ex tumore-recovered E12E cells. (A) Experimental regimen. BMT was performed as explained for Fig. 1 and followed by i.v. administration of 10^6 E12E cells and intraplantar infection with 10^5 PFU of mCMV-WT. After 7 weeks, E12E.surv cells (cells that have survived the apoptotic crisis) were recovered from relapsed, macroscopically visible tumor noduli (~3 mm in diameter), expanded in cell culture by three passages in the presence of G418, and transferred i.v. into 7-Gy-γ-irradiated indicator recipients. (B) Early kinetics of E12E.surv tumor growth. At the indicated time points after transfer of 10^6 E12E.surv cells, liver-resident IHC-stained CD45R$^+$ tumor cells were counted in representative 50-mm^2 areas of liver tissue sections. Dots represent data from individual recipients per time point and group (closed circles, indicator recipients infected with 10^5 PFU of mCMV-WT; open circles, uninfected indicator recipients) with the calculated log-linear regression lines indicated.

start (Fig. 12B1). Lack of apoptosis beyond day 4 (Fig. 9D) predicts that the apoptotic signal is no longer present on day 5 or later. Thus, the tumor cells should remain unaffected if administered later than on day 4 after infection. However, the kinetics clearly showed an antitumoral effect, and thus the continuance of the apoptotic signal, after an intraplantar infection performed 5 or even 6 days prior to administration of the tumor cells (Fig. 12B2). It is important to note that the time span between γ irradiation and administration of the tumor cells was found to have no influence on tumor growth, except that γ irradiation should precede the tumor for immunosuppression.

Collectively, these data lead us to propose that the tumor relapse after the apoptotic crisis reflects a programmed acquisition of reversible resistance by the tumor cell colonies rather than a cessation of the virally induced, apoptosis-triggering signal. In theory, this resistance could be a molecular property due to gene expression reprogramming in the individual tumor cell, a lack of accessibility of tumor cells protected within colonies, or even an active antiapoptotic defense exerted by colonies that exceed a critical size.

Activated NK cells fail in controlling the E12E lymphoma upon adoptive transfer. It has been frequently asked whether residual innate immunity (38) that resisted the 7-Gy hematoablative treatment might be involved in the antitumoral mechanism. Infection with mCMV has been reported to be a particularly strong inducer of IFN-α/β and interleukin-12, which systemically activate NK cells for cytotoxic activity and IFN-γ production, respectively (50). TNF-α, which is also induced by mCMV and which inhibits NK cell cytotoxicity while promoting IFN-γ production (50), has previously been shown to be uninvolved in the antitumoral mechanism of mCMV (24).

To evaluate the immunocompromising effect of 7-Gy γ irradiation on systemic NK cell activation by mCMV infection, we compared the NK cell content and functional activity in

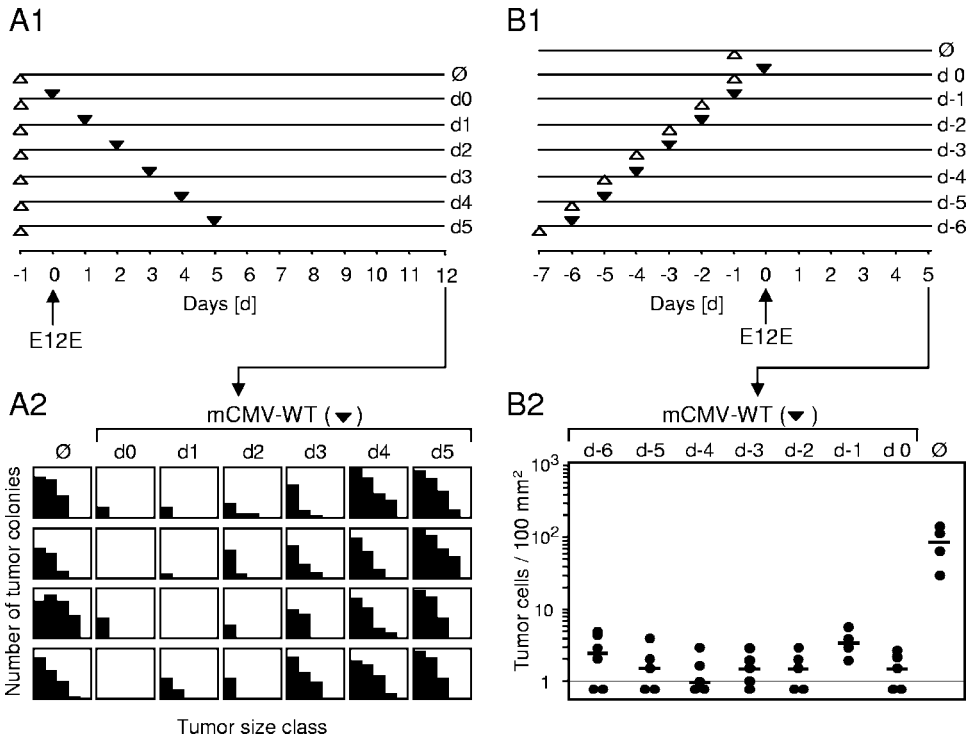

FIG. 12. Acquisition of resistance by developing E12E cell colonies. (A) Kinetics of the in vivo susceptibility of E12E lymphoma cells to virus-induced apoptosis. (A1) Experimental design. E12E cells were administered i.v. into immunocompromised indicator recipients according to the protocol explained for Fig. 3A. Recipient mice either were left uninfected (group ∅), were infected with mCMV-WT shortly after tumor cell transfer (group d0), or were infected with a delay increasing from 24 h (group d1) to 5 days (group d5). Time points of infection and of 7-Gy γ irradiation are indicated by closed and open arrowheads, respectively. (A2) For all groups, tumor burden in the liver was assessed on day 12 as explained for Fig. 3A, except that quantitation was based on 100 mm^2 of liver tissue sections. Size-frequency diagrams are shown for four individual recipients per group. (B) Continuance of the apoptotic environment after infection. (B1) Experimental design. Intravenous administration of E12E cells into immunocompromised mice was performed shortly after infection (group d 0) or was preceded by infection for 24 h (group d-1) to 6 days (group d-6). A control group immunocompromised on day −1 received tumor cells on day 0 but was left uninfected (group ∅). Time points of infection and of 7-Gy γ irradiation are indicated by closed and open arrowheads, respectively. (B2) For all groups, tumor burden in the liver was assessed after 5 days of tumor growth. This early time point was imposed by CMV disease in the groups with the most advanced infection. Dots represent tumor burden in representative 100-mm^2 areas of liver tissue sections of individual recipients. The median values are marked.

draining popliteal lymph nodes of immunocompetent and immunocompromised BALB/c mice on day 4 after infection with mCMV-WT; this corresponds to the time at which tumor cell apoptosis occurred in the liver of immunocompromised and infected tumor recipients. In the immunocompetent mice, the yield of cells from a popliteal lymph node was found to be in the order of magnitude of 10^7 cells, of which 3.6% in the particular experiment shown in Fig. 13 displayed the phenotype $CD49b^+$ $TCR\alpha/\beta^-$, which is characteristic of NK cells (4). Notably, these virus-sensitized lymph node cells lysed the prototypical NK target lymphoma cell YAC-1 as well as E12E cells, the B-cell lymphoma under investigation. This lytic activity could be attributed to the NK cells by its abrogation after depletion of $CD49b^+$ cells from the sensitized lymph node cell population. In contrast, at day 4 after infection of mice immunocompromised by a 7-Gy γ irradiation, the yield of lymph node cells was 100-fold less, namely, in the order of magnitude of 10^5 cells per popliteal lymph node. Of these, only 2.4% were found to display the NK cell phenotype $CD49b^+$ $TCR\alpha/\beta^-$, and their lytic activity was at best minimal at a very high effector-to-target cell ratio. It is worth noting that the radiation-resistant $TCR\alpha/\beta^+$ cells visible in the cytofluorometric analysis mainly represented $CD4^+$ T cells (not shown). In conclusion, contrary to the prediction of relative radiation resistance of NK cells, the data did not reveal any absolute or relative enrichment of activated $CD49b^+$ $TCR\alpha/\beta^-$ NK cells in 7-Gy-γ-irradiated and mCMV-infected BALB/c mice but rather indicated that the few remaining NK cells were functionally impaired. The data thus did not give evidence for a significant systemic NK cell activity in immunocompromised and infected tumor recipients.

It is obvious that a draining lymph node represents only a minor fraction of the total body pool of residual NK cells and that cytolytic activity might become measurable at extremely high effector-to-target cell ratios. Instead of trying to collect more NK cells from the immunocompromised and infected mice, we decided to use the straightforward approach of adoptive transfer for testing the antitumoral capacity of the strong NK cell activity that was actually present in the activated lymph node cell population of infected, immunocompetent mice used as adoptive transfer donors (Fig. 13, left panel). Specifically, 10^5 presensitized 4-day lymph node cells of immunocompetent and infected donors were transferred into immunocompromised indicator recipients that had received E12E cells 2 days

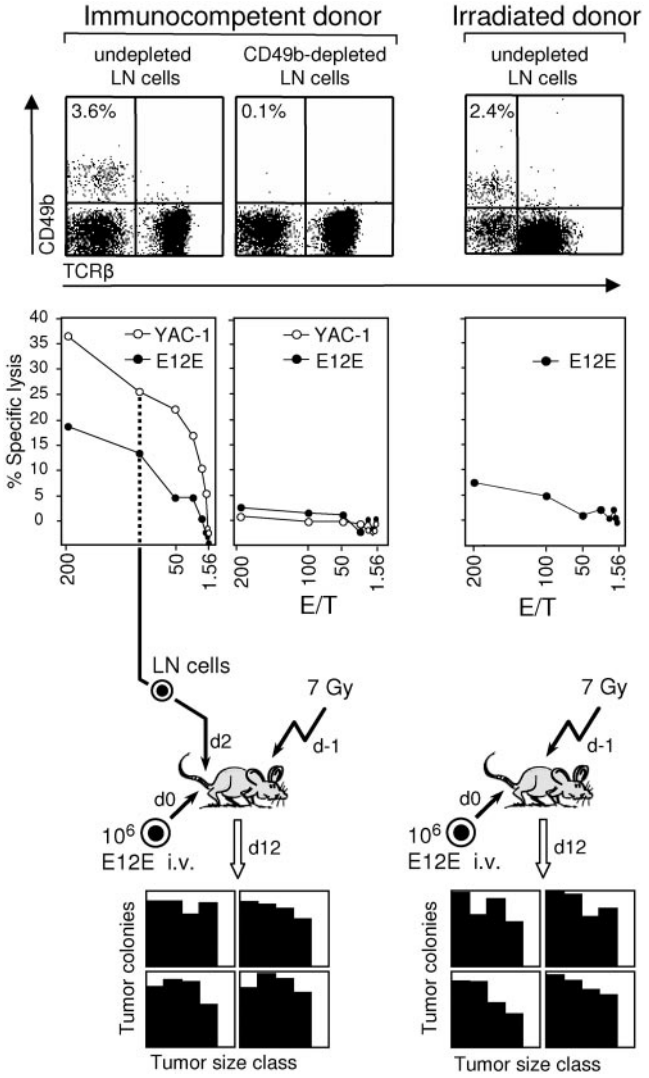

FIG. 13. Tumor-lytic NK cells fail to control E12E lymphoma growth in the liver. LN cells from the popliteal LN were isolated on day 4 after intraplantar infection with 10^5 PFU of mCMV-WT of either 7-Gy-γ-irradiated (n = 30 LNs; 8.4×10^4 cells per LN) or immunocompetent (n = 5 LNs; 8.6×10^6 cells per LN) BALB/c mice. An aliquot of the LN cells from the immunocompetent donors was depleted of CD49b-expressing cells by negative immunomagnetic cell sorting. (Top panel) Two-color cytofluorometric analysis of the expression of CD49b and TCR β-chain. The proportion of $CD49b^+TCR^-$ NK cells is indicated in the upper left quadrants. Data are shown by two-dimensional dot plots with 30,000 cells analyzed and 5,000 cells (dots) displayed. (Center panel) Lytic activity of the LN cells against E12E lymphoma cells and the prototypic NK-sensitive YAC-1 lymphoma cells at the effector-to-target cell ratios (E/T) indicated. Dots represent mean values of triplicate assay cultures. (Bottom panel) Undepleted day 4 LN cells (10^5) (corresponding to an effector-to-target cell ratio of 100) derived from the infected, immunocompetent donors were transferred i.v. into immunocompromised mice at day 2 after i.v. administration of 10^6 E12E lymphoma cells. Recipients with no LN cell transfer served as a control. Each lymphoma size-frequency diagram (CD45R IHC staining) for four individual recipients per group represents 100 mm^2 of liver tissue sections on day 12.

earlier. While in this protocol intraplantar infection can still control the tumor (recall Fig. 12A), the transferred NK cell activity did not show any inhibition of E12E lymphoma growth in the liver.

Collectively, this set of data did not provide evidence to suggest a role for systemically activated, extrahepatic NK cells in the control of the E12E lymphoma in the liver of the immunocompromised host.

DISCUSSION

In previous work, we have reported on the discovery of an unpredicted novel function of CMV, namely, the inhibition of a B-cell lymphoma in an experimental setting of hematoablative therapy followed by BMT in the mouse model (24). Although the effect was impressive in terms of survival benefit and a macroscopically prominent reduction of tumor mass, the underlying mechanism remained enigmatic. Several suggestive first-guess explanations, including a role for TNF-α, were ruled out, and based on experimental evidence, viral triggering of tumor cell apoptosis had been among the dismissed ideas. Specifically, in livers in which the E12E lymphoma and productive mCMV infection coincided, tumor cells located in intimate proximity to infected hepatocytes showed no cytopathological signs of apoptosis and did not express active caspase 3 but instead proliferated, as evidenced by mitotic figures and expression of proliferating cell nuclear antigen, a polymerase processivity factor indicative of growing cells. Although these data now proved to be absolutely correct for a late phase of tumor growth in the infected liver, the interpretation has to be revised in part. Here we have performed a detailed investigation into the kinetics of lymphoma growth in the presence of infection, with the surprising result that mCMV inhibits lymphoma growth by early induction of an apoptotic crisis and consequent transient tumor remission, after which surviving tumor cells account for tumor relapse in the presence of productive liver tissue infection with all the features discussed above and described precisely in our original report (24). To the best of our knowledge, such an antitumoral mechanism is without precedent in the literature. The sequence of events and synopsis of our current knowledge is illustrated in a model that is subdivided into three phases for sorting of our ideas and for discussion (Fig. 14).

Phase I: tumor cell extravasation, homing in tissue, and initial exponential growth. Under the conditions of the experiments, namely, a systemic intravenous administration of the lymphoma cells followed shortly thereafter by a peripheral subcutaneous/intraplantar infection, lymphoma cells successfully migrated through the endothelium at interendothelial junctions (5), settled down in the liver parenchyma, and started to proliferate until they reached the four-cell stage. As shown in Fig. 9, these early events occurred with no difference in uninfected and infected recipients. Leaving the circulation is a critical step for tumor cell survival and tumor metastasis (69, 70). Specifically, the half-life of E12E in the circulation was found to be only ~50 min. It is therefore instructive to get an estimate of how many of the administered E12E lymphoma cells actually populated the liver. This information can be gained from the transmigration rate revealed from the ordinate intercept of the log-linear in vivo growth curves. In the specific case of the uninfected group in Fig. 9B, the estimate was 15 transmigrated E12E cells in a unit area of 50 mm^2 that encompasses $\sim 2 \times 10^5$ nucleated liver tissue cells. Based on DNA content, a mouse liver consists of $\sim 3.5 \times 10^8$ cells, which

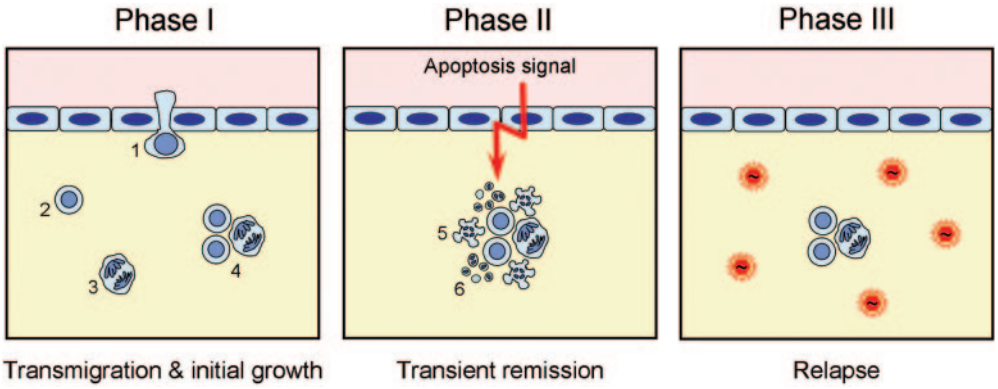

FIG. 14. Concluding model. See text in Discussion for a detailed explanation. A layer of endothelial cells separates the vascular/sinusoidal compartment (rose colored) and the intrahepatic compartment (yellow). Lymphoma cells are pictured in stages of endothelial transmigration (1), interphase (2), mitosis (3), small colony formation (4), and apoptosis (5) and as apoptotic bodies/vesicles (6). The red virus symbols indicate productive infection of liver parenchyma.

gives an estimate of ~25,000 transmigrated E12E cells for the whole liver, that is, ~2.5% of the 10^6 E12E cells administered intravenously. In other words, only 1 out of 40 lymphoma cells was successful in homing to the liver, but this rate was not influenced by the infection.

Phase II: transient tumor remission by induction of tumor cell apoptosis. Between days 2 and 5, tumor cell numbers declined in the infected group due to tumor cell apoptosis peaking on days 3 and 4. As we have learned from the size-frequency distribution analysis of tumor colonies on day 5 (Fig. 10), 95% of the tumor colonies were wiped out by apoptosis during this period, and in the remaining colonies the cell numbers declined because the rate of apoptosis exceeded the rate of proliferation. We would predict that the probability for an extinction of the lymphoma increases under conditions of a lower initial tumor cell burden and hence of a lower number of transmigrating cells colonizing the liver. This view is supported by the improved survival benefit gained by the infection, as documented in Fig. 1 for lower initial numbers of tumor cells. In this phase of tumor remission by apoptosis, productive infection of liver tissue by mCMV-WT is still at the detection limit (Fig. 7A1); moreover, as has been shown with the dissemination-deficient mutant mCMV-ΔM36, infection of the liver is not a condition for lymphoma inhibition. We therefore propose an apoptosis-triggering signal or death ligand that is induced by a distant infection. Importantly, since apoptosis was not observed in hepatocytes, this virally induced, long-range proapoptotic signal appears to target the tumor cells selectively.

Phase III: tumor relapse by exponential growth of surviving tumor cells. Beyond day 5, surviving tumor cells proliferated with an unaltered doubling time. This indicated that tumor cells either were eliminated during the apoptotic crisis in phase II or survived essentially undamaged. By serial transfer of cells from relapsed tumor noduli, we have ruled out a selection of apoptosis-resistant, genetically stable E12E variants during the remission phase under a selective force exerted by the apoptosis-triggering signal. In accordance with the idea of a programmed acquisition of resistance by advanced tumor colonies, for instance by reaching a critical size or by reprogrammed gene expression in adaptation to host tissue stroma, resistance against the virally induced proapoptotic signal was found to be acquired also in the absence of infection. Once resistant or protected, tumor cells continued to proliferate even in the presence of a full-blown and tissue-destroying liver infection. This is the situation described in our original report (24). It is inherent to the rules of exponential growth that a reduction in the number of tumor cells during the transient remission slows down the progress of tumor growth, and this explains the dramatic differences in absolute tumor burden and median survival times observed later on.

Pending questions. While we have now identified transient remission by tumor cell apoptosis as the eventual effector mechanism of the mCMV-induced inhibition of tumor growth, apparent questions are open to future investigation.

First, what is the virus-specific molecular signal or death receptor ligand that is induced by distantly replicating mCMV, as shown here for mCMV-WT and the dissemination-deficient mutant mCMV-ΔM36 but not by the related alphaherpesviruses HSV-1 and HSV-2? It could be a secreted "virokine" encoded by a gene that is not conserved between mCMV and HSVs, which would most easily explain the observed virus specificity. Infection with a random transposon insertion library of mCMV is a theoretically conceivable approach successfully used previously to identify genes for which a phenotype existed in cell culture (for an overview, see reference 15). However, the effort of screening a very large number of mutant viruses for loss of an antitumoral effect in vivo is on a different scale. Whereas CMVs are well known to employ antiapoptotic and prosurvival proteins to prolong cell survival for efficient virus replication (references 3, 13, 14, and 48; for reviews, see references 30 and 62), proapoptotic functions are scarcely noted and less well defined. Data suggesting that mCMV infection induces apoptosis in uninfected "bystander" cells specifically in neuronal tissues have been reported (43, 60, 71). As we have never detected expression of active caspase 3 in uninfected hepatocytes adjacent to foci of productive infection in the liver (Podlech, unpublished data), there appears to exist a cell type selectivity. In accordance with this, we have shown here apoptotic lymphoma cells located within apparently nonapoptotic liver parenchyma (Fig. 9C).

A tumor-preferential induction of apoptosis is reminiscent of TRAIL/Apo2L (1, 32), a member of the cellular TNF cyto-

kine family, as well as of the viral proteins adenovirus e4ORF4 (11) and chicken anemia virus Apoptin/VP3 (49); of these proteins, however, only TRAIL operates by inducing a cell-extrinsic death receptor pathway (reviewed in reference 61), whereas e4ORF4 and Apoptin/VP3 operate only within infected tumor cells. Since mCMV does not infect E12E lymphoma cells, only a TRAIL-related mechanism could apply. Thus, as an alternative to a virus-encoded trigger of apoptosis, mCMV infection might induce the expression of a secreted cellular TRAIL-like death receptor ligand in the infected cells, or possibly also indirectly through cytokines in uninfected cells. Although infection regulates numerous cellular genes, the virus specificity gives a reasonable chance to identify candidates by a differential mouse expression microarray analysis. Since it has been reported for the parental A20 B-cell lymphoma model that TRAIL/Apo2L gene-deficient BALB/c mice show an increased lymphoma load in the liver (64), murine TRAIL/Apo2L is a promising candidate. A problem arises, however, from the fact that our data suggest a long-range effect likely mediated by a soluble protein induced at an extrahepatic site of virus replication, whereas murine TRAIL/Apo2L is a membrane protein expressed on cytokine-stimulated NK cells (40), including activated hepatic-derived NK cells (66, 67). Although we have presented experimental evidence here against a critical role for innate immunity mediated by residual $CD49b^+$ $TCR\alpha/\beta^-$ extrahepatic NK cells, at present we cannot rule out an involvement of radiation-resistant liver-specific NK cells, the so-called pit cells, in the virally induced apoptotic crisis. Thus, a long-range viral or virus-induced signal, for instance IFN-α/β and/or interleukin-12 (50), could systemically stimulate the liver-resident NK/pit cells to mediate tumor cell apoptosis locally. Our approach of NK cell transfer (Fig. 13) did not rule out a role for liver-specific NK/pit cells, since intravenously transferred lymph node-derived NK cells must first migrate through the sinusoidal endothelium and may thus not necessarily substitute for liver-resident NK/pit cells that are already located in the intrahepatic, transendothelial compartment within the perisinusoidal space of Disse.

Another puzzle is why the apoptosis is only transient. One possibility was that the postulated virus-encoded or virus-induced death signal comes as a wave and then vanishes, for instance due to eradication of the death ligand-expressing/secreting cells by cytolytic infection. Continuation of an antitumoral environment beyond day 4 after infection (Fig. 12B), that is, during the relapse phase III, strongly argues against cessation of the apoptotic signal. Instead, Fig. 12A shows that tumor cells growing in the liver of uninfected mice lose susceptibility to the apoptotic signal when they reach the 64-cell stage. We thus propose that the tumor colonies acquire a programmed, reversible resistance against the death signal.

One idea is that cells in the interior of advanced tumor noduli are sterically shielded from the apoptotic signal as a sort of "barricade defense." However, on day 5 in the infected group, which corresponds to a calculated 32-cell stage, apoptotic cells were no longer detectable (Fig. 9D), although cell loss by preceding apoptosis had reduced the actual number of surviving cells in these colonies (Fig. 10). It therefore appears to us unconvincing to propose that the apoptotic signal no longer reached the tumor cells; at least cells at the periphery of the colonies should have been accessible. However, no apoptotic cells at all were detected on day 5. Another possibility, although somewhat speculative at the moment, is that colonies that have reached a critical size take active measures of defense to neutralize apoptotic signals.

We currently favor the hypothesis that the tumor cells acquire intrinsic resistance against the death signal, for instance by downmodulation of the corresponding death receptor. This could be a programmed event associated with tumor cell homing to tissue stroma and, possibly, the beginning of angiogenesis. Importantly, this phenotypic switch is apparently not linked to cell cycle control, as it occurs during exponential growth. A hint may be given by the expression of reporter gene *lacZ*. The reporter gene was originally integrated into E12E cells to allow their detection in situ but never came to use because it was found to be rapidly silenced in vivo. β-Galactosidase-negative lymphoma cells that were recovered from tumor noduli still contained the *lacZ* gene and expressed it after desilencing during a few cell culture passages (Erlach, unpublished data). In a new interpretation, silencing of the reporter gene may have in fact reported a more general gene silencing event that takes place in young tumor cell colonies at the ~32-cell stage and also silences genes involved in susceptibility to apoptosis. Conversely, reprogramming of gene expression in developing tumor colonies may also desilence previously silenced genes involved in resistance to apoptosis, possibly including the expression of decoy receptors for Apo2L/TRAIL, of FLIP, or of IAPs (*i*nhibitor of *a*poptosis *p*roteins) (for a detailed discussion, see reference 1).

In conclusion, we have here identified transient tumor cell apoptosis as the effector mechanism by which mCMV inhibits lymphoma growth, and we have precisely defined the time window of tumor cell susceptibility. As shown in Fig. 3B, the antitumoral effect of mCMV is not restricted to A20 and A20-derived B-cell lymphomas but also applies to T-cell lymphomas. So, we are looking for a mechanism of broader relevance. The aim of future work will be to identify the death ligand and receptor pair that triggers the virus-induced apoptosis.

ACKNOWLEDGMENTS

Support to J.P. and M.J.R. was provided by the Deutsche Forschungsgemeinschaft, Collaborative Research grant SFB 432, "Mechanisms of tumor defense and their therapeutic implications," individual project A10, "Influence of cytomegalovirus infection on the risk of leukemia relapse after bone marrow transplantation."

We thank Jens Martin Knabe, Anette Denner, and Petra Deegen for expert technical contributions and assistance; Rafaela Holtappels (SFB 490, E3) for advice regarding CMV immunology; and Susanne Strand (SFB 432, B6) for advice regarding apoptosis. Michael Reddehase greatly helped us with the linear regression analysis. We are particularly indebted to Ulrich H. Koszinowski, Peter Ghazal, Martin Messerle, and Ana Angulo for the possibility to work with virus mutants mCMV-ΔM36 and mCMV-ΔMIEenh. T-cell lymphoma cell lines ESb-MP and ESb-L-CI were generously provided by Volker Schirrmacher, German Cancer Research Centre, Heidelberg, Germany.

REFERENCES

1. **Almasan, A., and A. Ashkenazi.** 2003. Apo2L/TRAIL: apoptosis signaling, biology, and potential for cancer therapy. Cytokine Growth Factor Rev. **14:**337–348.
2. **Alterio de Goss, M., R. Holtappels, H.-P. Steffens, J. Podlech, P. Angele, L. Dreher, D. Thomas, and M. J. Reddehase.** 1998. Control of cytomegalovirus in bone marrow transplantation chimeras lacking the prevailing antigen-presenting molecule in recipient tissues rests primarily on recipient-derived CD8 T cells. J. Virol. **72:**7733–7744.
3. **Andoniou, C. E., D. M. Andrews, M. Manzur, P. Ricciardi-Castagnoli, and**

M. A. Degli-Esposti. 2004. A novel checkpoint in the Bcl-2-regulated apoptotic pathway revealed by murine cytomegalovirus infection of dendritic cells. J. Cell Biol. **166:**827–837.
4. **Arase, H., T. Saito, J. H. Phillips, and L. L. Lanier.** 2001. Cutting edge: the mouse NK cell-associated antigen recognized by DX5 monoclonal antibody is CD49b (a2 integrin, very late antigen-2). J. Immunol. **167:**1141–1144.
5. **Aurrand-Lions, M., C. Johnson-Leger, and B. A. Imhof.** 2002. The last molecular fortress in leukocyte trans-endothelial migration. Nat. Immunol. **3:**116–118.
6. **Benke, R., and V. Schirrmacher.** 1991. Change in organotropism of mouse lymphoma variants associated with selective chemotactic responsiveness to organ-derived chemoattractants. Clin. Exp. Metastasis **9:**205–219.
7. **Benyesh-Melnick, M., P. A. Schaffer, R. J. Courtney, J. Esparza, and S. Kimura.** 1975. Viral gene functions expressed and detected by temperature-sensitive mutants of herpes simplex virus. Cold Spring Harbor Symp. Quant. Biol. **39:**731–746.
8. **Blaheta, R. A., W. D. Beecken, T. Engl, D. Jonas, E. Oppermann, M. Hundemer, H. W. Doerr, M. Scholz, and J. Cinatl.** 2004. Human cytomegalovirus infection of tumor cells downregulates NCAM (CD56): a novel mechanism for virus-induced tumor invasiveness. Neoplasia **6:**323–331.
9. **Boeckh, M., W. G. Nichols, G. Papanicolaou, R. Rubin, J. R. Wingard, and J. Zaia.** 2003. Cytomegalovirus in hematopoietic stem cell transplant recipients: current status, known challenges, and future strategies. Biol. Blood Marrow Transplant. **9:**543–558.
10. **Boehme, K. W., and T. Compton.** 2006. Virus entry and activation of innate immunity, p. 111–130. *In* M. J. Reddehase (ed.), Cytomegaloviruses: molecular biology and immunology. Caister Academic Press, Norfolk, United Kingdom.
11. **Branton, P. E., and D. E. Roopchand.** 2001. E4ORF4 protein in viral replication and cell killing. Oncogene **20:**7855–7865.
12. **Bruggemann, M., C. Pott, M. Ritgen, and M. Kneba.** 2004. Significance of minimal residual disease in lymphoid malignancies. Acta Haematol. **112:**111–119.
13. **Brune, W., C. Menard, J. Heesemann, and U. H. Koszinowski.** 2001. A ribonucleotide reductase homolog of cytomegalovirus and endothelial cell tropism. Science **291:**303–305.
14. **Brune, W., M. Nevels, and T. Shenk.** 2003. Murine cytomegalovirus m41 open reading frame encodes a Golgi-localized antiapoptotic protein. J. Virol. **77:**11633–11643.
15. **Brune, W., M. Wagner, and M. Messerle.** 2006. Manipulating cytomegalovirus genomes by BAC mutagenesis: strategies and applications, p. 63–89. *In* M. J. Reddehase (ed.), Cytomegaloviruses: molecular biology and immunology. Caister Academic Press, Norfolk, United Kingdom.
16. **Campana, D.** 2004. Minimal residual disease studies in acute leukemia. Am. J. Clin. Pathol. **122:**S47–S57.
17. **Castagnola, E., B. Cappelli, D. Erba, A. Rabagliati, E. Lanino, and G. Dini.** 2004. Cytomegalovirus infection after bone marrow transplantation in children. Hum. Immunol. **65:**416–422.
18. **Cicin-Sain, L., J. Podlech, M. Messerle, M. J. Reddehase, and U. H. Koszinowski.** 2005. Frequent coinfection of cells explains functional in vivo complementation between cytomegalovirus variants in the multiply infected host. J. Virol. **79:**9492–9502.
19. **Cobbs, C. S., L. Harkins, M. Samanta, G. Y. Gillespie, S. Bharara, P. H. King, L. B. Nabors, C. G. Cobbs, and W. J. Britt.** 2002. Human cytomegalovirus infection and expression in human malignant glioma. Cancer Res. **62:**3347–3350.
20. **Doninger, J., S. Muralidhar, and L. J. Rosenthal.** 1999. Human cytomegalovirus and human herpesvirus 6 genes that transform and transactivate. Clin. Microbiol. Rev. **12:**367–382.
21. **Egorov, I. K.** 2006. Mouse models of efficient and inefficient anti-tumor immunity, with emphasis on minimal residual disease and tumor escape. Cancer Immunol. Immunother. **55:**1–22.
22. **Einsele, H., and H. Hebart.** 2004. CMV-specific immunotherapy. Hum. Immunol. **65:**558–564.
23. **Erlach, K. C.** 2003. Influence of cytomegalovirus infection on the risk of leukemia relapse after bone marrow transplantation. Ph.D. thesis. Johannes Gutenberg-University, Mainz, Germany.
24. **Erlach, K. C., J. Podlech, A. Rojan, and M. J. Reddehase.** 2002. Tumor control in a model of bone marrow transplantation and acute liver-infiltrating B-cell lymphoma: an unpredicted novel function of cytomegalovirus. J. Virol. **76:**2857–2870.
25. **Falke, D.** 1965. Untersuchungen über die Beziehungen zwischen Riesenzellbildung und Infektiosität von Herpes simplex Virus. Arch. Ges. Virusforsch. **15:**387–401.
26. **Field, H. J., and P. Wildy.** 1978. The pathogenicity of thymidine kinase-deficient mutants of herpes simplex virus in mice. J. Hyg. **81:**267–277.
27. **Fujiwara, H., Y. Eizuru, T. Matsumoto, T. Kukita, R. Imaizumi, H. Kawada, H. Ohtsubo, K. Matsushita, N. Arima, and C. Tei.** 2001. The significance of cytomegalovirus infection over the clinical course of adult T-cell leukemia/lymphoma. Microbiol. Immunol. **45:**97–100.
28. **Fujiwara, H., T. Matsumoto, Y. Eizuru, K. Matsushita, H. Ohtsubo, T. Kukita, R. Imaizumi, M. Matsumoto, S. Hidaka, N. Arima, and C. Tei.** 2000. Cytomegalovirus infection is not necessarily a poor prognostic factor in adult T-cell leukemia/lymphoma. J. Med. Virol. **62:**140–143.
29. **Ghazal, P., M. Messerle, K. Osborn, and A. Angulo.** 2003. An essential role of the enhancer for murine cytomegalovirus in vivo growth and pathogenesis. J. Virol. **77:**3217–3228.
30. **Goldmacher, V. S.** 2005. Cell death suppression by cytomegaloviruses. Apoptosis **10:**251–265.
31. **Grzimek, N. K. A., J. Podlech, H.-P. Steffens, R. Holtappels, S. Schmalz, and M. J. Reddehase.** 1999. In vivo replication of recombinant murine cytomegalovirus driven by the paralogous major immediate-early promoter-enhancer of human cytomegalovirus. J. Virol. **73:**5043–5055.
32. **Gura, T.** 1997. How TRAIL kills cancer cells, but not normal cells. Science **277:**768.
33. **Hebart, H., and H. Einsele.** 2004. Clinical aspects of CMV infection after stem cell transplantation. Hum. Immunol. **65:**432–436.
34. **Holtappels, R., M. W. Munks, J. Podlech, and M. J. Reddehase.** 2006. CD8 T cell-based immunotherapy of cytomegalovirus disease in the mouse model of the immunocompromised bone marrow transplantation recipient, p. 383–418. *In* M. J. Reddehase (ed.), Cytomegaloviruses: molecular biology and immunology. Caister Academic Press, Norfolk, United Kingdom.
35. **Holtappels, R., M.-F. Pahl-Seibert, D. Thomas, and M. J. Reddehase.** 2000. Enrichment of immediate-early 1 (*m123*/pp89) peptide-specific CD8 T cells in a pulmonary $CD62L^{lo}$ memory-effector cell pool during latent murine cytomegalovirus infection of the lungs. J. Virol. **74:**11495–11503.
36. **Holtappels, R., J. Podlech, G. Geginat, H.-P. Steffens, D. Thomas, and M. J. Reddehase.** 1998. Control of murine cytomegalovirus in the lungs: relative but not absolute immunodominance of the immediate-early 1 nonapeptide during the antiviral cytolytic T-lymphocyte response in pulmonary infiltrates. J. Virol. **72:**7201–7212.
37. **Holtappels, R., J. Podlech, N. K. A. Grzimek, D. Thomas, M.-F. Pahl-Seibert, and M. J. Reddehase.** 2001. Experimental preemptive immunotherapy of murine cytomegalovirus disease with CD8 T-cell lines specific for ppM83 and pM84, the two homologs of human cytomegalovirus tegument protein ppUL83 (pp65). J. Virol. **75:**6584–6600.
38. **Jonjic, S., I. Bubic, and A. Krmpotic.** 2006. Innate immunity to cytomegaloviruses, p. 285–319. *In* M. J. Reddehase (ed.), Cytomegaloviruses: molecular biology and immunology. Caister Academic Press, Norfolk, United Kingdom.
39. **Jurianz, K., P. von Hoegen, and V. Schirrmacher.** 1999. Immunological and molecular characterization of an aggressive murine lymphoma variant: modulation in vitro and in vivo. Int. J. Oncol. **15:**71–79.
40. **Kayagaki, N., N. Yamaguchi, M. Nakayama, K. Takeda, H. Akiba, H. Tsutsui, H. Okamura, K. Nakanishi, K. Okumura, and H. Yagita.** 1999. Expression and function of TNF-related apoptosis-inducing ligand on murine activated NK cells. J. Immunol. **163:**1906–1913.
41. **Kim, K. J., C. Kanellopoulos-Langevin, R. M. Merwin, D. H. Sachs, and R. Asofsky.** 1979. Establishment and characterization of BALB/c lymphoma lines with B cell properties. J. Immunol. **122:**549–554.
42. **Kohlhage, H., and R. Siegert.** 1962. Zwei genetisch determinierte Varianten eines Herpes-simplex-Stammes. Arch. Ges. Virusforsch. **12:**273–286.
43. **Kosugi, I., Y. Shinmura, R.-Y. Li, S. Aiba-Masago, S. Baba, K. Miura, and Y. Tsutsui.** 1998. Murine cytomegalovirus induces apoptosis in non-infected cells of the developing mouse brain and blocks apoptosis in primary neuronal culture. Acta Neuropathol. **96:**239–247.
44. **Krüger, A., V. Schirrmacher, and P. von Hoegen.** 1994. Scattered micrometastases visualized at the single-cell level: detection and re-isolation of lacZ-labeled metastasized lymphoma cells. Int. J. Cancer **58:**275–284.
45. **Kurz, S., H.-P. Steffens, A. Mayer, J. R. Harris, and M. J. Reddehase.** 1997. Latency versus persistence or intermittent recurrences: evidence for a latent state of murine cytomegalovirus in the lungs. J. Virol. **71:**2980–2987.
46. **Madrigal, J. A., I. Scott, R. Arguello, R. Szydlo, A. M. Little, and J. M. Goldman.** 1997. Factors influencing the outcome of bone marrow transplants using unrelated donors. Immunol. Rev. **157:**153–166.
47. **McKie, E. A., S. M. Brown, A. R. MacLean, and D. I. Graham.** 1998. Histopathological responses in the CNS following inoculation with a non-neurovirulent mutant (1716) of herpes simplex virus type 1 (HSV 1): relevance for gene and cancer therapy. Neuropathol. Appl. Neurobiol. **24:**367–372.
48. **Menard, C., M. Wagner, Z. Ruzsics, K. Holak, W. Brune, A. E. Campbell, and U. H. Koszinowski.** 2003. Role of murine cytomegalovirus US22 gene family members in replication in macrophages. J. Virol. **77:**5557–5570.
49. **Noteborn, M. H. M., A. A. A. M. Danen-van Oorschot, and A. J. Van der Eb.** 1998. Chicken anemia virus: induction of apoptosis by a single protein of a single-stranded DNA virus. Semin. Virol. **8:**497–504.
50. **Orange, J. S., and C. A. Biron.** 1996. Characterization of early IL-12, IFN-alphabeta, and TNF effects on antiviral state and NK cell responses during murine cytomegalovirus infection. J. Immunol. **156:**4746–4756.
51. **Pahl-Seibert, M.-F., M. Juelch, J. Podlech, D. Thomas, P. Deegen, M. J. Reddehase, and R. Holtappels.** 2005. Highly protective in vivo function of cytomegalovirus IE1 epitope-specific memory CD8 T cells purified by T-cell receptor-based cell sorting. J. Virol. **79:**5400–5413.

52. **Plachter, B., C. Sinzger, and G. Jahn.** 1996. Cell types involved in replication and distribution of human cytomegalovirus. Adv. Virus Res. **46:**195–261.
53. **Podlech, J., R. Holtappels, N. K. A. Grzimek, and M. J. Reddehase.** 2002. Animal models: murine cytomegalovirus. Methods Microbiol. **32:**493–525.
54. **Podlech, J., R. Holtappels, M.-F. Pahl-Seibert, H.-P. Steffens, and M. J. Reddehase.** 2000. Murine model of interstitial cytomegalovirus pneumonia in syngeneic bone marrow transplantation: persistence of protective pulmonary CD8-T-cell infiltrates after clearance of acute infection. J. Virol. **74:** 7496–7507.
55. **Podlech, J., R. Holtappels, N. Wirtz, H.-P. Steffens, and M. J. Reddehase.** 1998. Reconstitution of CD8 T cells is essential for the prevention of multiple-organ cytomegalovirus histopathology after bone marrow transplantation. J. Gen. Virol. **79:**2099–2104.
56. **Podlech, J., K. Weise, and D. Falke.** 1990. Colonization of adrenal glands and ovaries of mice by HSV-2 variants. I. Virological studies. Arch. Virol. **110:** 165–177.
57. **Rapp, F.** 1984. Cytomegalovirus and carcinogenesis. J. Natl. Cancer Inst. **72:**783–787.
58. **Reddehase, M. J.** 2002. Antigens and immunoevasins: opponents in cytomegalovirus immune surveillance. Nat. Rev. Immunol. **2:**831–844.
59. **Reddehase, M. J., J. B. Rothbard, and U. H. Koszinowski.** 1989. A pentapeptide as minimal antigenic determinant for MHC class I-restricted T lymphocytes. Nature (London) **337:**651–653.
60. **Reuter, J. D.** 2005. Cytomegalovirus induces T-cell independent apoptosis in brain during immunodeficiency. J. Clin. Virol. **32:**218–223.
61. **Rohn, J. L., and M. H. M. Noteborn.** 2004. The viral death effector Apoptin reveals tumor-specific processes. Apoptosis **9:**315–322.
62. **Sanchez, V., and D. H. Spector.** 2006. Exploitation of host cell cycle regulatory pathways by HCMV, p. 205–230. *In* M. J. Reddehase (ed.), Cytomegaloviruses: molecular biology and immunology. Caister Academic Press, Norfolk, United Kingdom.
63. **Scholz, M., R. A. Blaheta, B. Wittig, J. Cinatl, J.-U. Vogel, H. W. Doerr, and J. Cinatl, Jr.** 2000. Cytomegalovirus-infected neuroblastoma cells exhibit augmented invasiveness mediated by b1a5 integrin (VLA-5). Tissue Antigens **55:**412–421.
64. **Sedger, L. M., M. B. Glaccum, J. C. L. Schuh, S. T. Kanaly, E. Williamson, N. Kayagaki, T. Yun, P. Smolak, T. Le, R. Goodwin, and B. Gliniak.** 2002. Characterization of the in vivo function of TNF-a-related apoptosis-inducing ligand, TRAIL/Apo2L, using TRAIL/Apo2L gene-deficient mice. Eur. J. Immunol. **32:**2246–2254.
65. **Simon, C. O., C. K. Seckert, D. Dreis, M. J. Reddehase, and N. K. A. Grzimek.** 2005. Role for tumor necrosis factor alpha in murine cytomegalovirus transcriptional reactivation in latently infected lungs. J. Virol. **79:**326–340.
66. **Smyth, M. J., E. Cretney, K. Takeda, R. H. Wiltrout, L. M. Sedger, N. Kayagaki, H. Yagita, and K. Okumura.** 2001. Tumor necrosis factor-related apoptosis-inducing ligand (TRAIL) contributes to interferon-gamma-dependent natural killer cell protection from tumor metastasis. J. Exp. Med. **193:**661–670.
67. **Takeda, K., Y. Hayakawa, M. J. Smyth, N. Kayagaki, N. Yamaguchi, S. Kakuta, Y. Iwakura, H. Yagita, and K. Okumura.** 2001. Involvement of tumor necrosis factor-related apoptosis-inducing ligand in surveillance of tumor metastasis by liver natural killer cells. Nat. Med. **7:**94–100.
68. **Timbury, M. C.** 1971. Temperature-sensitive mutants of herpes simplex virus type 2. J. Gen. Virol. **13:**373–376.
69. **Weiss, L., F. W. Orr, and K. V. Honn.** 1989. Interactions between cancer cells and the microvasculature: a rate-regulator for metastasis. Clin. Exp. Metastasis **7:**127–167.
70. **Weiss, L., and G. W. Schmid-Schönbein.** 1989. Biomechanical interactions of cancer cells with the microvasculature during metastasis. Cell Biophys. **14:** 187–215.
71. **Zhang, M., and S. S. Atherton.** 2002. Apoptosis in the retina during MCMV retinitis in immunosuppressed BALB/c mice. J. Clin. Virol. **25**(Suppl. 2)**:** S137–S147.